

Article

Magnesium-Doped $\text{Sr}_2(\text{Fe},\text{Mo})\text{O}_{6-\delta}$ Double Perovskites with Excellent Redox Stability as Stable Electrode Materials for Symmetrical Solid Oxide Fuel Cells

Kun Zheng ^{1,2,*} , Jakub Lach ¹, Hailei Zhao ^{3,4} , Xiubing Huang ³ and Kezhen Qi ⁵ 

¹ Department of Hydrogen Energy, Faculty of Energy and Fuels, AGH University of Science and Technology, al. A. Mickiewicza 30, 30-059 Krakow, Poland

² AGH Centre of Energy, AGH University of Science and Technology, ul. Czarnowiejska 36, 30-054 Krakow, Poland

³ School of Materials Science and Engineering, University of Science and Technology Beijing, Beijing 100083, China

⁴ Beijing Key Lab of New Energy Materials and Technology, Beijing 100083, China

⁵ College of Pharmacy, Dali University, Dali 671000, China

* Correspondence: zheng@agh.edu.pl

Abstract: In this work, magnesium-doped $\text{Sr}_2\text{Fe}_{1.2}\text{Mg}_{0.2}\text{Mo}_{0.6}\text{O}_{6-\delta}$ and $\text{Sr}_2\text{Fe}_{0.9}\text{Mg}_{0.4}\text{Mo}_{0.7}\text{O}_{6-\delta}$ double perovskites with excellent redox stability have been successfully obtained. The physicochemical properties including: crystal structure properties, redox stability, thermal expansion properties in oxidizing and reducing conditions, oxygen content as a function of temperature and transport properties, as well as the chemical compatibility with typical electrolytes have been systematically investigated. The in situ oxidation of reduced samples using high-temperature XRD studies shows the crystal structure of materials stable at up to a high-temperature range. The in situ reduction and oxidation of sinters with dilatometer measurements prove the excellent redox stability of materials, with the thermal expansion coefficients measured comparable with electrolytes. The oxygen nonstoichiometry δ of compounds was determined and recorded in air and argon up to 900 °C. $\text{Sr}_2\text{Fe}_{1.2}\text{Mg}_{0.2}\text{Mo}_{0.6}\text{O}_{6-\delta}$ oxide presents satisfactory values of electrical conductivity in air ($56.2 \text{ S}\cdot\text{cm}^{-1}$ at 600 °C) and reducing conditions ($10.3 \text{ S}\cdot\text{cm}^{-1}$ at 800 °C), relatively high coefficients D and k , and good ionic conductivity (cal. $0.005 \text{ S}\cdot\text{cm}^{-1}$ at 800 °C). The stability studies show that both compounds are compatible with $\text{Ce}_{0.8}\text{Gd}_{0.2}\text{O}_{1.9}$ but react with the $\text{La}_{0.8}\text{Sr}_{0.2}\text{Ga}_{0.8}\text{Mg}_{0.2}\text{O}_{3-d}$ electrolyte. Therefore, the magnesium-doped double perovskites with excellent redox stability can be potentially qualified as electrode materials for symmetrical SOFCs and are of great interest for further investigations.

Keywords: Mg-doped $\text{Sr}_2\text{Fe}_{1.2}\text{Mg}_{0.2}\text{Mo}_{0.6}\text{O}_{6-\delta}$ and $\text{Sr}_2\text{Fe}_{0.9}\text{Mg}_{0.4}\text{Mo}_{0.7}\text{O}_{6-\delta}$ double perovskites; excellent redox-stable electrode materials; thermal expansion; oxygen content as a function of temperature; transport properties; symmetrical solid oxide fuel cells



Citation: Zheng, K.; Lach, J.; Zhao, H.; Huang, X.; Qi, K. Magnesium-Doped $\text{Sr}_2(\text{Fe},\text{Mo})\text{O}_{6-\delta}$ Double Perovskites with Excellent Redox Stability as Stable Electrode Materials for Symmetrical Solid Oxide Fuel Cells. *Membranes* **2022**, *12*, 1006. <https://doi.org/10.3390/membranes12101006>

Academic Editor: V. María Barragán

Received: 26 September 2022

Accepted: 14 October 2022

Published: 18 October 2022

Publisher's Note: MDPI stays neutral with regard to jurisdictional claims in published maps and institutional affiliations.



Copyright: © 2022 by the authors. Licensee MDPI, Basel, Switzerland. This article is an open access article distributed under the terms and conditions of the Creative Commons Attribution (CC BY) license (<https://creativecommons.org/licenses/by/4.0/>).

1. Introduction

Energy generation by the combustion of fossil fuels (coal, oil, and their derivatives) brings various serious environmental issues, and the depletion of these fuels urgently requires the development of new alternative clean and green energy sources. Solid Oxide Fuel Cells (SOFCs) are among the most promising technologies for the production of electricity and heat from traditional and renewable energy sources [1–8]. The main advantage of SOFCs is their high efficiency and fuel flexibility. They can also significantly reduce CO_2 emissions and other harmful gases (NO_x , SO_x , CO) when compared to traditional combustion technology. However, when the mostly available carbon-containing cheap fuels are applied in SOFCs, carbon deposition over the anode occurs and, in consequence, significantly decreases the power output. Those fuels usually contain a small amount of sulfur, which causes the sulfur poisoning problem (even at a level of several ppm of H_2S) at the

anode and greatly deteriorates the cell performance. The application of symmetrical Solid Oxide Fuel Cells (S-SOFCs) with identical electrode material can easily eliminate or lessen the coking and sulfur poisoning issues by simply changing the gas flow. The traditional cell configuration with three components (anode, electrolyte, cathode) can be replaced by a new approach, where the same electrode material could be used simultaneously as both a cathode and anode to construct a S-SOFC. The symmetrical cells are very promising, due to the reduced amount of cell components, a simplification of the manufacturing process, and by reducing the problems associated with the chemical stability of materials, which, in consequence, will either reduce production costs or ensure a long-term stable operation of SOFCs. Another important benefit related with the application of S-SOFCs will be the ability to address the sulfur poisoning and carbon deposition problems by simply reversing the gas flows when SOFCs are fueled by cheap and available non-hydrogen fuels. In addition, such a symmetrically constructed cell facilitates a reversible operation between fuel cell mode and electrolysis mode. Since the S-SOFC concept was first proposed by a patent of Badding et al. in 2001 [9] and peer-reviewed in articles [10,11] in 2006, it has drawn on a lot of intensive research on the search for novel electrode materials for S-SOFC cells. Furthermore, NASA has developed a novel S-SOFC design with thin YSZ electrolytes using a novel ceramic fabrication technique, generating a good performance ($\sim 900 \text{ mW cm}^{-2}$) at $850 \text{ }^\circ\text{C}$ [12]. Recently, the very good electrochemical performance of S-SOFCs with redox-stable electrode materials has been reported [13,14]. However, excellent power outputs exceeding 1000 mW cm^{-2} of S-SOFCs are recorded, rather, at high temperature ranges (around $800 \text{ }^\circ\text{C}$) [15–19]. To lower the operating temperature of S-SOFCs while still maintaining a high power output, electrodes with highly active and stable materials are required.

The application of redox-stable double perovskites as electrode materials in S-SOFCs seems to be particularly of interest [14–16]. One group of the most interesting electrode materials for SOFCs is the B-site Mo-containing perovskite. The Mo-containing anode materials possess very promising SOFC performance in hydrogen and methane fuels [4,20–22]. In particular, Fe- and Mo-containing $\text{Sr}_{2-x}\text{Ba}_x\text{MMoO}_6$ ($\text{M} = \text{Mg}, \text{Mn}, \text{Fe}, \text{Co}, \text{Ni}$) double perovskite-type oxides, with B-site rock salt-type ordering, are of great interest [23–27]. The present redox pair of $\text{Fe}^{2+}/\text{Fe}^{3+}$ and $\text{Mo}^{6+}/\text{Mo}^{5+}$ in $\text{Sr}_2(\text{Fe},\text{Mo})\text{O}_{6-\delta}$ -type perovskites can provide not only enhanced conductivity [24,25], but also excellent redox stability both in reducing and oxidizing the atmosphere [28–30]. In general, the chemical composition consideration in $\text{Sr}_2(\text{Fe},\text{Mo})\text{O}_{6-\delta}$ -type double perovskites is guarded by several criteria. The big difference in the oxidation state of cations between Mo^{6+} or Mo^{5+} (in reducing conditions) and bigger M (*3d* metals, Mg) metals having typically +2 or +3 ensures an appearance of a double perovskite structure with the B-site cations-ordering [4,31]. Moreover, such a mixed valence configuration ($\text{Mo}^{6+}/\text{Mo}^{5+}$ and $\text{M}^{2+}/\text{M}^{3+}$) favors an effective charge transport and also facilitates the creation of oxygen vacancies in materials. $\text{Sr}_2(\text{Fe},\text{Mo})\text{O}_{6-\delta}$ double perovskite presents metallic conductivity properties while exceeding 1000 S cm^{-1} conductivity in 5 vol.% H_2/Ar , while unfortunately, the material is not stable in an oxidizing condition [24]. $\text{SrFe}_{0.75}\text{Mo}_{0.25}\text{O}_{3-\delta}$ [28,29], $\text{SrFe}_{0.5}\text{Mn}_{0.25}\text{Mo}_{0.25}\text{O}_{3-\delta}$ [28], and $\text{Sr}_{1-x}\text{Ba}_x\text{Fe}_{0.75}\text{W}_{0.25}\text{O}_{3-\delta}$ [32] perovskites show good redox stability and have been evaluated as novel anode materials for S-SOFCs fueled by methane or CO. However, $\text{Sr}_2\text{Fe}_{1.5}\text{Mo}_{0.5}\text{O}_{6-\delta}$ is sensitive to water, and the reaction with water at low temperatures is a potential shortcoming of this material for application in SOFCs [33,34]. The double perovskite $(\text{PrBa})_{0.95}(\text{Fe}_{0.9}\text{Mo}_{0.1})_2\text{O}_{5+\delta}$ shows very good conductivity of 217 S cm^{-1} in air and 59.2 S cm^{-1} in 5% H_2 at $800 \text{ }^\circ\text{C}$ [18]. In addition, the electrode is structurally stable in various fuels, suggesting that the cell can be operated in flexible gas conditions [17]. Interestingly, SOFC cells with $(\text{PrBa})_{0.95}(\text{Fe}_{0.9}\text{Mo}_{0.1})_2\text{O}_{5+\delta}$ anodes also show outstanding performance in H_2S -containing fuel (1.18 W cm^{-2} @ $800 \text{ }^\circ\text{C}$ in $\text{H}_2+100\text{ppmH}_2\text{S}$), which indicates this material also has excellent tolerance to sulfur poisoning [18]. The copper-doped $\text{Sr}_2\text{Fe}_{1.5}\text{Mo}_{0.3}\text{Cu}_{0.2}\text{O}_{6-\delta}$ oxide with enhanced reaction activity and durability was studied for the electrochemical oxidation of H_2 and reduction of CO_2 ,

showing a peak SOFC power output of 1.51 W cm^{-2} in hydrogen and a current density of 1.94 A cm^{-2} at 1.4 V in the reduction of CO_2 to CO [35]. Ti-doped $\text{Sr}_2\text{Fe}_{1.4-x}\text{Ti}_x\text{Mo}_{0.6}\text{O}_{6-\delta}$ double perovskites with an improved structural stability ascribed to the strong Ti-O bond were studied as novel anode materials for SOFCs, with $\text{Sr}_2\text{Fe}_{1.3}\text{Ti}_{0.1}\text{Mo}_{0.6}\text{O}_{6-\delta}$ anode-based cells delivering a very good power density exceeding 0.64 W cm^2 at $900 \text{ }^\circ\text{C}$ in humidified H_2 [36]. $\text{Sr}_2\text{TiNi}_{0.5}\text{Mo}_{0.5}\text{O}_{6-\delta}$ was also proposed as a potential oxide anode for SOFCs [37]. $\text{Sr}_2\text{FeMo}_{2/3}\text{Mg}_{1/3}\text{O}_{6-\delta}$ double perovskite due to the presence of $\text{Fe}_B\text{-O-Fe}_B'$ bonds promoting the easy formation and fast migration of oxygen vacancies in the lattice was proposed as a promising anode material for SOFCs with a good tolerance to carbon deposition and sulfur poisoning [38]. However, the very low electrical conductivity in air ($4\text{--}5 \text{ S cm}^{-1}$ in air $600\text{--}800 \text{ }^\circ\text{C}$) makes the application of such a compound as a cathode material almost impossible [38]. The effects of Co and Mo doping on the properties of the $\text{SrFe}_{0.45}\text{Co}_{0.45}\text{Mo}_{0.1}\text{O}_{3-\delta}$ perovskite as an air electrode in reversible solid oxide cells have been investigated [39]. The small bond strength of Co-O contributes to the high mobility of both electron holes and oxide ions, while leading to a high thermal expansion coefficient for the Co-doped composition [39]. $\text{Sr}_2\text{Mg}_{1-x}\text{Co}_x\text{MoO}_{6-\delta}$ compounds were proposed as anode materials for SOFCs, and the Co-substitution positively affects the sinterability and ionic conductivity, thus decreasing the anode polarization resistance [40]. However, the weak bond of Co-O causes the stability problem due to the reduction in cobalt to metallic Co in anode conditions. In general, the good transport properties of Fe- and Mo-containing double perovskites can be very promising electrode material candidates for S-SOFCs [18,19,28,29,41].

In this work, magnesium-doped $\text{Sr}_2\text{Fe}_{1.2}\text{Mg}_{0.2}\text{Mo}_{0.6}\text{O}_{6-\delta}$ and $\text{Sr}_2\text{Fe}_{0.9}\text{Mg}_{0.4}\text{Mo}_{0.7}\text{O}_{6-\delta}$ double perovskites have been evaluated as potential redox-stable electrode materials for S-SOFCs. The chemical composition of $\text{Sr}_2\text{Fe}_{1.2}\text{Mg}_{0.2}\text{Mo}_{0.6}\text{O}_{6-\delta}$ and $\text{Sr}_2\text{Fe}_{0.9}\text{Mg}_{0.4}\text{Mo}_{0.7}\text{O}_{6-\delta}$ has been selected in order to provide good redox stability and electrical conductivity of materials in reducing and oxidizing conditions. The magnesium doping in the proposed compounds can potentially enhance the redox stability, and the content of Mo contributes to the good electrical conductivity [24,28,36,38]. In this study, the physicochemical properties, including the phase composition, crystal structure and its evolution on temperature, redox stability, thermal expansion properties in oxidizing and reducing conditions, oxygen nonstoichiometry and transport properties, as well as chemical stability with electrolytes have been systematically studied.

2. Experimental

$\text{Sr}_2\text{Fe}_{1.2}\text{Mg}_{0.2}\text{Mo}_{0.6}\text{O}_{6-\delta}$ and $\text{Sr}_2\text{Fe}_{0.9}\text{Mg}_{0.4}\text{Mo}_{0.7}\text{O}_{6-\delta}$ materials were synthesized by the high-temperature solid state reaction method, with calculated stoichiometric amounts of SrCO_3 , Fe_2O_3 , MgO , and MoO_3 (all with $\geq 99.9\%$ purity) compounds as initial chemicals. All needed chemicals were milled in a high-efficiency Spex Sample-Prep 8000 M planetary ball mill, and afterwards, the well-milled powders were pressed into pellets and sintered at $1200 \text{ }^\circ\text{C}$ for 10 h in air. The crystal structure of the obtained samples was characterized by XRD measurements using a Panalytical Empyrean diffractometer in the $10\text{--}110 \text{ deg}$ range with $\text{CuK}\alpha$ radiation. The redox stability of the studied materials was investigated by the reduction in compounds in 5 vol.% H_2/Argon at $1000 \text{ }^\circ\text{C}$ for 10 h. The in situ oxidation of the reduced $\text{Sr}_2\text{Fe}_{1.2}\text{Mg}_{0.2}\text{Mo}_{0.6}\text{O}_{6-\delta}$ and $\text{Sr}_2\text{Fe}_{0.9}\text{Mg}_{0.4}\text{Mo}_{0.7}\text{O}_{6-\delta}$ compounds in air was studied by the high-temperature XRD (HT-XRD) measurements performed on a Panalytical Empyrean apparatus equipped with an Anton Paar HTK 1200N oven-chamber. The collected XRD data were refined with the Rietveld method applying the GSAS/EXPGUI software [42,43].

The in situ reduction and oxidation of the investigated sinters were conducted with the thermal expansion studies in 5 vol.% H_2/Argon and air up to $900 \text{ }^\circ\text{C}$ on a Linseis L75 Platinum Series dilatometer. Thermogravimetric (TG) analysis was conducted on the TA Instruments Q5000IR apparatus from room temperature (RT) up to $900 \text{ }^\circ\text{C}$, with a heating rate of $2^\circ \cdot \text{min}^{-1}$ in different atmospheres (air and argon). The buoyancy effect was also appropriately considered. The oxygen nonstoichiometry δ of $\text{Sr}_2\text{Fe}_{1.2}\text{Mg}_{0.2}\text{Mo}_{0.6}\text{O}_{6-\delta}$ and

$\text{Sr}_2\text{Fe}_{0.9}\text{Mg}_{0.4}\text{Mo}_{0.7}\text{O}_{6-\delta}$ oxides was determined by the iodometric titration method at RT, and the experimental details can be found in [44]. The titration measurement was performed on an EM40-BNC Mettler Toledo titrator furnished with a platinum electrode. The oxygen nonstoichiometry δ of materials was calculated by using the average values from three independent titration experiments. The total electrical conductivity of the studied compounds was measured up to 900 °C in air and 5 vol.% H_2/Ar by a four-probe DC method for measuring electrical conductivity (σ). Experiments were performed on dense cuboid shape samples (approx. 3 mm × 4 mm × 10 mm). The porosity effect of the sinters was taken into consideration, with an appropriate correction taken from Bruggeman's effective medium approximation [45]. The oxygen diffusion coefficient D and surface exchange coefficient k of $\text{Sr}_2\text{Fe}_{1.2}\text{Mg}_{0.2}\text{Mo}_{0.6}\text{O}_{6-\delta}$ oxide were also evaluated by the mass relaxation technique using TA Instruments Q5000 IR apparatus on thin-sheet shape sinter [46,47]. The mass relaxation data were collected during the rapid change of oxygen partial pressure between 0.21 atm and 0.01 atm. The calculation of the chemical diffusion coefficient D and surface exchange constant k was performed in a custom-made Matlab code, based on mathematical solutions provided by Crank [48]. The chemical stability and compatibility studies of $\text{Sr}_2\text{Fe}_{1.2}\text{Mg}_{0.2}\text{Mo}_{0.6}\text{O}_{6-\delta}$ and $\text{Sr}_2\text{Fe}_{0.9}\text{Mg}_{0.4}\text{Mo}_{0.7}\text{O}_{6-\delta}$ oxides towards typical solid electrolytes CGO20 ($\text{Ce}_{0.8}\text{Gd}_{0.2}\text{O}_{1.9}$) and LSGM ($\text{La}_{0.8}\text{Sr}_{0.2}\text{Ga}_{0.8}\text{Mg}_{0.2}\text{O}_{3-d}$) were examined by analyzing the XRD data collected for the respective oxide and the electrolyte powder mixtures (50:50 wt.%), which were annealed at 1200 °C for 4 h in air.

3. Results and Discussion

3.1. Crystal Structure and the Redox Stability

Figure 1a,b show the XRD patterns with the Rietveld refinement of the as-synthesized $\text{Sr}_2\text{Fe}_{1.2}\text{Mg}_{0.2}\text{Mo}_{0.6}\text{O}_{6-\delta}$ and $\text{Sr}_2\text{Fe}_{0.9}\text{Mg}_{0.4}\text{Mo}_{0.7}\text{O}_{6-\delta}$ compounds, which were sintered for 10 h at 1200 °C in air. Both samples exhibit a B-site double perovskite structure with an $Fm-3m$ space group, and no other impurities can be observed in the detection limit. A similar double perovskite structure ($Fm-3m$ space group) has also been reported for $\text{Sr}_2\text{FeMo}_{2/3}\text{Mg}_{1/3}\text{O}_{6-\delta}$ [38], Ti-doped $\text{Sr}_2\text{Fe}_{1.4-x}\text{Ti}_x\text{Mo}_{0.6}\text{O}_{6-\delta}$ ($x = 0$ and 0.1) [36], and $\text{Sr}_2\text{Fe}_{1.5}\text{Mo}_{0.5}\text{O}_{6-\delta}$ oxides [29]. Interestingly, $\text{Sr}_2\text{FeMoO}_{6-\delta}$ [24] and $\text{Sr}_2\text{MgMoO}_{6-\delta}$ [49] oxides possess lower symmetry with the $I4/m$ and $I-1$ space groups, respectively. The structural parameters based on the Rietveld refinement results of the studied materials are presented in Table 1. The increased content of magnesium doping in materials leads to the increase in unit cell parameter a from 7.8604 Å (for $\text{Sr}_2\text{Fe}_{1.2}\text{Mg}_{0.2}\text{Mo}_{0.6}\text{O}_{6-\delta}$) to 7.8709 Å (for $\text{Sr}_2\text{Fe}_{0.9}\text{Mg}_{0.4}\text{Mo}_{0.7}\text{O}_{6-\delta}$), which is due to the large ionic radius of Mg^{2+} ($r_{\text{Mg}^{2+}} = 0.72$ Å). As the $\text{Sr}_2\text{Fe}_{1.2}\text{Mg}_{0.2}\text{Mo}_{0.6}\text{O}_{6-\delta}$ and $\text{Sr}_2\text{Fe}_{0.9}\text{Mg}_{0.4}\text{Mo}_{0.7}\text{O}_{6-\delta}$ double perovskites were synthesized in the air, the presence of $\text{Fe}^{3+}/\text{Fe}^{4+}$ ($r_{\text{Fe}^{3+}} = 0.645$ Å and $r_{\text{Fe}^{4+}} = 0.585$ Å) and Mo^{6+} ($r_{\text{Mo}^{6+}} = 0.59$ Å) should be dominant. Therefore, the doping of the much larger Mg^{2+} in the studied materials should increase the unit cell parameters as observed in Table 1. The geometric tolerance factor t_g was also calculated with the equation $t_g = \frac{[\text{A}-\text{O}]}{\sqrt{2}[\text{B}-\text{O}]}$, where $[\text{A}-\text{O}]$ and $[\text{B}-\text{O}]$ are the appropriate geometric averages of the refined interatomic distances of Sr-O and M-O (M: Fe, Mg and Mo), respectively [24]. The tolerance factors t_g calculated for $\text{Sr}_2\text{Fe}_{1.2}\text{Mg}_{0.2}\text{Mo}_{0.6}\text{O}_{6-\delta}$ and $\text{Sr}_2\text{Fe}_{0.9}\text{Mg}_{0.4}\text{Mo}_{0.7}\text{O}_{6-\delta}$ oxides are 1.00 and 0.963, respectively.

As the electrode materials for S-SOFCs working both in the oxidization and reduction of the atmosphere, the redox stability of investigated samples is very crucial. $\text{Sr}_2\text{Fe}_{1.2}\text{Mg}_{0.2}\text{Mo}_{0.6}\text{O}_{6-\delta}$ and $\text{Sr}_2\text{Fe}_{0.9}\text{Mg}_{0.4}\text{Mo}_{0.7}\text{O}_{6-\delta}$ were reduced in 5 vol.% H_2/Argon at 1000 °C for 10 h, and the XRD patterns are presented in Figure 1c,d, which show the redox stability of Mg-doped materials. The reduced samples present the same crystal structure ($Fm-3m$), while the unit cell parameters a slightly increase (see Table 1). This is related to the reduction of $\text{Fe}^{3+}/\text{Fe}^{4+}$ to $\text{Fe}^{3+}/\text{Fe}^{2+}$ and Mo^{6+} to $\text{Mo}^{5+}/\text{Mo}^{4+}$ [28]. Interestingly, the relative unit cell volume change ΔV between the reduced and oxidized samples is very small, and the increased Mg-doping content decreases the volume change ΔV (Figure 2), which is associated with the redox-stable Mg^{2+} and the decreased content of Fe with change-

able oxidation states in the sample. In particular, the $\text{Sr}_2\text{Fe}_{0.9}\text{Mg}_{0.4}\text{Mo}_{0.7}\text{O}_{6-\delta}$ compound possesses a very small volume change, $\Delta V = 0.55\%$, which favors the application of such a material both in reducing and oxidizing conditions [46]. For comparison, the relative volume change between the reduced and oxidized $\text{Sr}_2\text{Fe}_{1.5}\text{Mo}_{0.5}\text{O}_{6-\delta}$ oxide is much larger and reaches 1.18% [28].

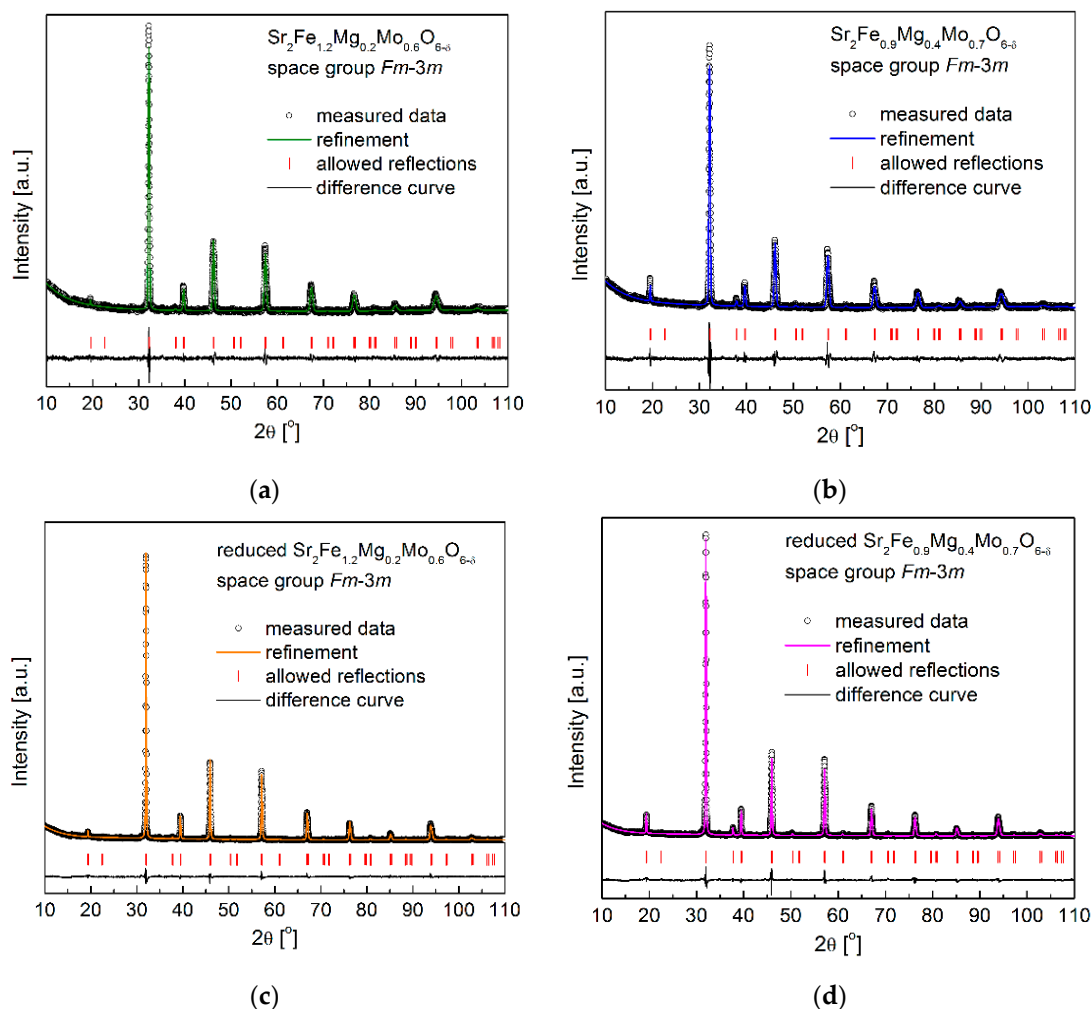


Figure 1. XRD patterns recorded for (a) as-synthesized $\text{Sr}_2\text{Fe}_{1.2}\text{Mg}_{0.2}\text{Mo}_{0.6}\text{O}_{6-\delta}$ and (b) $\text{Sr}_2\text{Fe}_{0.9}\text{Mg}_{0.4}\text{Mo}_{0.7}\text{O}_{6-\delta}$, (c) reduced $\text{Sr}_2\text{Fe}_{1.2}\text{Mg}_{0.2}\text{Mo}_{0.6}\text{O}_{6-\delta}$ and (d) $\text{Sr}_2\text{Fe}_{0.9}\text{Mg}_{0.4}\text{Mo}_{0.7}\text{O}_{6-\delta}$.

Table 1. Rietveld refinement results for as-synthesized and reduced $\text{Sr}_2\text{Fe}_{1.2}\text{Mg}_{0.2}\text{Mo}_{0.6}\text{O}_{6-\delta}$ and $\text{Sr}_2\text{Fe}_{0.9}\text{Mg}_{0.4}\text{Mo}_{0.7}\text{O}_{6-\delta}$ oxides.

Composition	$\text{Sr}_2\text{Fe}_{1.2}\text{Mg}_{0.2}\text{Mo}_{0.6}\text{O}_{6-\delta}$		$\text{Sr}_2\text{Fe}_{0.9}\text{Mg}_{0.4}\text{Mo}_{0.7}\text{O}_{6-\delta}$	
	as-Synthesized	Reduced at 1000 °C	as-Synthesized	Reduced at 1000 °C
T [°C]				
space group	<i>Fm-3m</i>	<i>Fm-3m</i>	<i>Fm-3m</i>	<i>Fm-3m</i>
<i>a</i> [Å]	7.8604(1)	7.8836(1)	7.8709(1)	7.8854(1)
<i>V</i> [Å ³]	485.67(1)	489.97(1)	487.61(1)	490.30(1)
density [g/cm ³]	5.48	5.43	5.43	5.40
R _p (%)	2.13	1.43	2.62	1.77
R _{wp} (%)	2.84	2.02	3.89	2.74

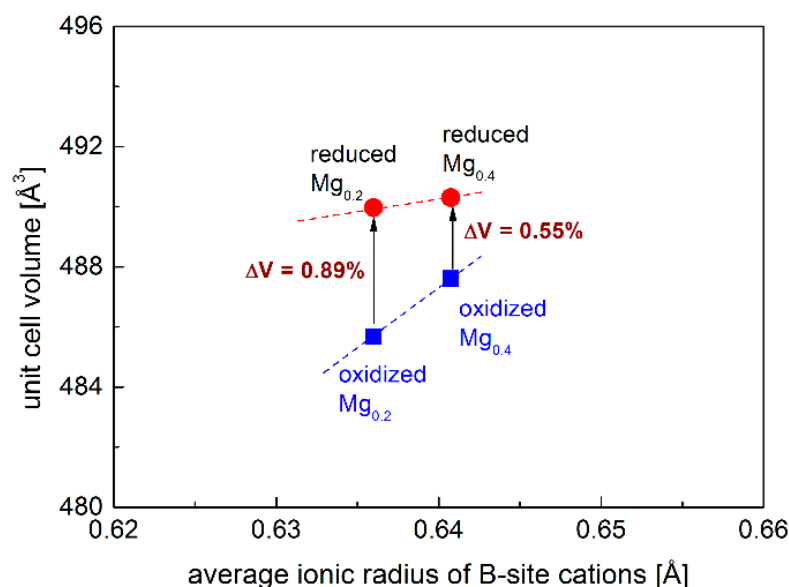


Figure 2. Normalized unit cell volume of reduced and oxidized $\text{Sr}_2\text{Fe}_{1.2}\text{Mg}_{0.2}\text{Mo}_{0.6}\text{O}_{6-\delta}$ ($\text{Mg}_{0.2}$), $\text{Sr}_2\text{Fe}_{0.9}\text{Mg}_{0.4}\text{Mo}_{0.7}\text{O}_{6-\delta}$ ($\text{Mg}_{0.4}$) as a function of B-site cations' ionic radius. Error values are smaller than the visible points. The average ionic radius of B-site cations was calculated only using the ionic radius of Fe^{3+} and Mo^{6+} cations for a direct comparison of the relative volume change of reduced and oxidized oxides.

For further studies of the redox stability of electrode materials, the reduced $\text{Sr}_2\text{Fe}_{1.2}\text{Mg}_{0.2}\text{Mo}_{0.6}\text{O}_{6-\delta}$ and $\text{Sr}_2\text{Fe}_{0.9}\text{Mg}_{0.4}\text{Mo}_{0.7}\text{O}_{6-\delta}$ samples were in situ oxidized in air utilizing HT-XRD measurements (Figure 3a–c). The lattice parameters of samples at different temperatures can be calculated by the Rietveld refinement of collected HT-XRD data, and the obtained unit cell parameter variations of the investigated compounds are depicted in Figure 3a. Firstly, the unit cell parameter a of both the two samples linearly increases with the temperature to 250 °C, showing the thermal expansion of reduced materials in this low temperature range. The significant (non-linear) change in the lattice parameter occurs at around 300 °C, indicating the oxidation of the reduced samples. The oxidation of the reduced samples causes the decrease in the unit cell parameter a , which is due to the oxidation of $\text{Fe}^{2+}/\text{Fe}^{3+}$ and $\text{Mo}^{4+}/\text{Mo}^{5+}$ to high oxidation states ($\text{Fe}^{3+}/\text{Fe}^{4+}$ and Mo^{6+}). The already oxidized materials show linear thermal expansion above 350 °C. The thermal expansion coefficients (TEC) of samples shown in the inset can be derived with the fitted linear slope. In general, the TECs obtained from the HT-XRD measurements for both the two materials are relatively low and in the range of $12.9\text{--}15.1 \times 10^{-6} \text{ K}^{-1}$. Those values are comparable with the TEC values of typical electrolytes [24], which indicates the possible good mechanical cohesion of electrode materials with electrolytes. For both the two materials, no phase transition has been observed, and the crystal structure with the $Fm\text{-}3m$ space group is stabilized up to 900 °C (Figure 3b,c).

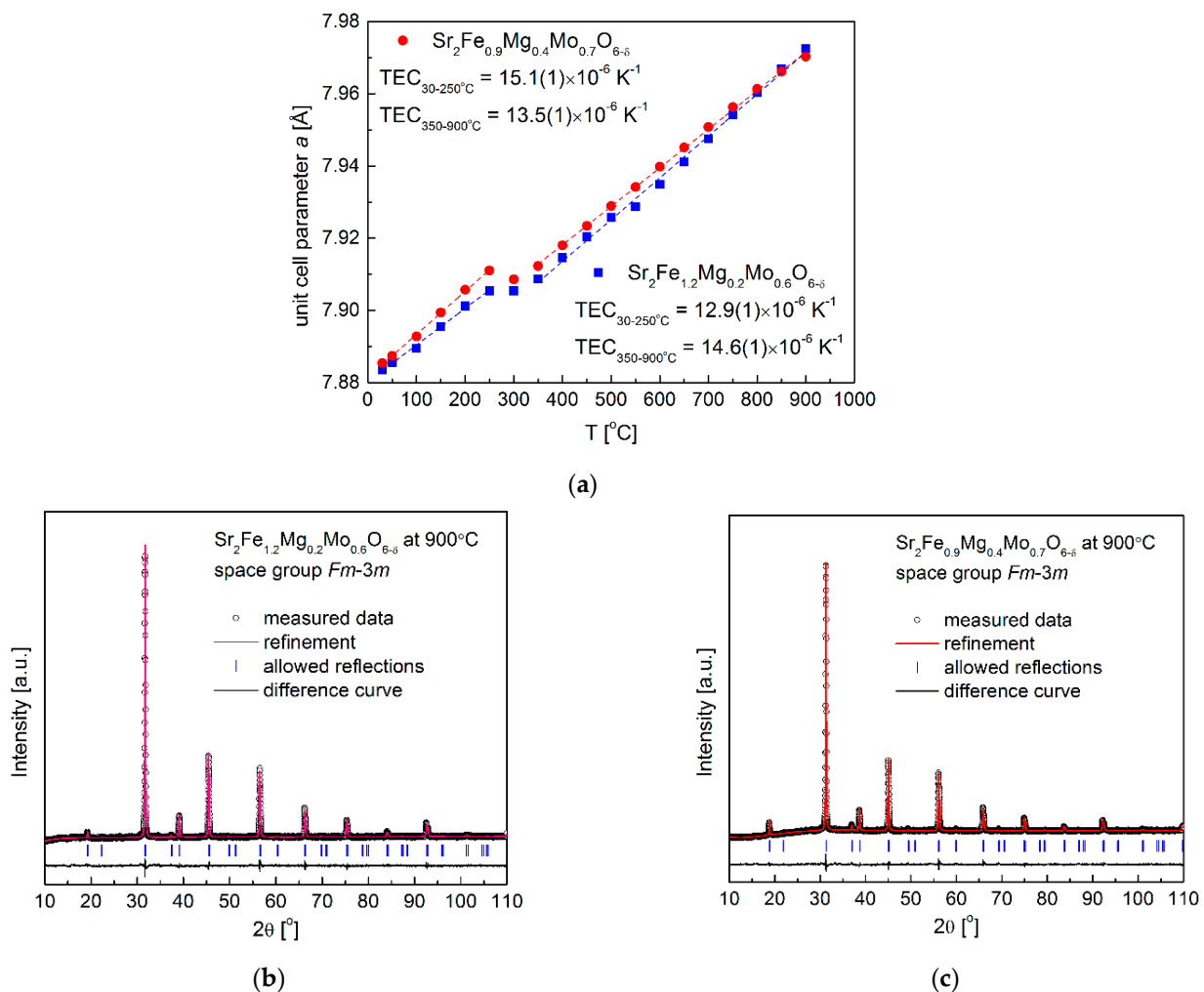


Figure 3. (a) In situ XRD measurements of oxidizing reduced $\text{Sr}_2\text{Fe}_{1.2}\text{Mg}_{0.2}\text{Mo}_{0.6}\text{O}_{6-\delta}$ and $\text{Sr}_2\text{Fe}_{0.9}\text{Mg}_{0.4}\text{Mo}_{0.7}\text{O}_{6-\delta}$ oxides in air from 30–900 °C, (b) XRD patterns recorded for $\text{Sr}_2\text{Fe}_{1.2}\text{Mg}_{0.2}\text{Mo}_{0.6}\text{O}_{6-\delta}$ and (c) $\text{Sr}_2\text{Fe}_{0.9}\text{Mg}_{0.4}\text{Mo}_{0.7}\text{O}_{6-\delta}$ samples at 900 °C in air.

3.2. Thermal Expansion Properties and Oxygen Nonstoichiometry

The in situ reduction and oxidation of $\text{Sr}_2\text{Fe}_{1.2}\text{Mg}_{0.2}\text{Mo}_{0.6}\text{O}_{6-\delta}$ and $\text{Sr}_2\text{Fe}_{0.9}\text{Mg}_{0.4}\text{Mo}_{0.7}\text{O}_{6-\delta}$ oxides were examined by applying dilatometer measurements (Figure 4a,b). In air, $\text{Sr}_2\text{Fe}_{1.2}\text{Mg}_{0.2}\text{Mo}_{0.6}\text{O}_{6-\delta}$ sample ($\text{TEC} = 15.6 \times 10^{-6} \text{ K}^{-1}$) shows slightly higher TEC values than $\text{Sr}_2\text{Fe}_{0.9}\text{Mg}_{0.4}\text{Mo}_{0.7}\text{O}_{6-\delta}$ ($\text{TEC} = 14.7 \times 10^{-6} \text{ K}^{-1}$), which indicates that the magnesium doping suppresses the thermal expansion of materials. In addition, the lower content of oxygen vacancies in $\text{Sr}_2\text{Fe}_{0.9}\text{Mg}_{0.4}\text{Mo}_{0.7}\text{O}_{6-\delta}$ also contributes to a smaller TEC than that of $\text{Sr}_2\text{Fe}_{1.2}\text{Mg}_{0.2}\text{Mo}_{0.6}\text{O}_{6-\delta}$. The in situ reduction in $\text{Sr}_2\text{Fe}_{1.2}\text{Mg}_{0.2}\text{Mo}_{0.6}\text{O}_{6-\delta}$ and $\text{Sr}_2\text{Fe}_{0.9}\text{Mg}_{0.4}\text{Mo}_{0.7}\text{O}_{6-\delta}$ samples were conducted by dilatometer studies in 5 vol.% H_2/Ar , and a linear thermal expansion of both materials as a function of temperature was documented up to around 400 °C. The continuous reduction of materials leads to a considerable expansion of the samples, which is associated with the reduction of $\text{Fe}^{3+}/\text{Fe}^{4+}$ and Mo^{6+} to low oxygen states, and a similar reduction behavior was also recorded in the TG measurements (Figure 5a,b). The significant reduction of Fe and Mo was up to 550 °C, while the further increase in the temperature contributed to a linear thermal expansion of the reduced samples. The reduced samples in 5 vol.% H_2/Ar possess relatively low thermal expansion values above 550 °C, with $14.6 \times 10^{-6} \text{ K}^{-1}$ for $\text{Sr}_2\text{Fe}_{1.2}\text{Mg}_{0.2}\text{Mo}_{0.6}\text{O}_{6-\delta}$ and $14.2 \times 10^{-6} \text{ K}^{-1}$ for $\text{Sr}_2\text{Fe}_{0.9}\text{Mg}_{0.4}\text{Mo}_{0.7}\text{O}_{6-\delta}$. Moreover, the reduced sinters were in situ oxidized in air with dilatometer measurements (Figure 4a,b). In the case of reduced $\text{Sr}_2\text{Fe}_{1.2}\text{Mg}_{0.2}\text{Mo}_{0.6}\text{O}_{6-\delta}$,

the linear thermal expansion is below 150 °C, while for $\text{Sr}_2\text{Fe}_{0.9}\text{Mg}_{0.4}\text{Mo}_{0.7}\text{O}_{6-\delta}$, the reduced sample linearly expands to around 200 °C, corresponding well with the linear expansion of the lattice parameters measured in the HT-XRD studies (Figure 3a). The continuous oxidation of reduced sinters leads to an interval shrinkage for the samples, which is due to the decrease in the unit cell parameters recorded in Figure 3a, caused by the oxidation of $\text{Fe}^{2+}/\text{Fe}^{3+}$ and $\text{Mo}^{4+}/\text{Mo}^{5+}$ to $\text{Fe}^{3+}/\text{Fe}^{4+}$ and Mo^{6+} . Above 400 °C, the samples are fully oxidized and show further linear expansion properties. The magnesium doping in $\text{Sr}_2\text{Fe}_{0.9}\text{Mg}_{0.4}\text{Mo}_{0.7}\text{O}_{6-\delta}$ ($\text{TEC} = 15.7 \times 10^{-6} \text{ K}^{-1}$) decreases the TEC value in the reducing condition when compared with $\text{Sr}_2\text{Fe}_{1.2}\text{Mg}_{0.2}\text{Mo}_{0.6}\text{O}_{6-\delta}$ sample. In general, $\text{Sr}_2\text{Fe}_{0.9}\text{Mg}_{0.4}\text{Mo}_{0.7}\text{O}_{6-\delta}$ oxide possesses smaller TEC values than $\text{Sr}_2\text{Fe}_{1.2}\text{Mg}_{0.2}\text{Mo}_{0.6}\text{O}_{6-\delta}$ (see Table 2). Therefore, Mg doping in materials suppresses the thermal expansion of samples in the oxidation and reduction of atmospheres. Importantly, for both the $\text{Sr}_2\text{Fe}_{1.2}\text{Mg}_{0.2}\text{Mo}_{0.6}\text{O}_{6-\delta}$ and $\text{Sr}_2\text{Fe}_{0.9}\text{Mg}_{0.4}\text{Mo}_{0.7}\text{O}_{6-\delta}$ compounds, no visible cracks were detected after the in situ reduction and oxidation studies by the dilatometer measurements, which proved the excellent redox stability of the investigated materials. The TEC values of the materials collected from the dilatometer studies and HT-XRD measurements in the oxidizing and reducing conditions are in the range of $12.9\text{--}15.7 \times 10^{-6} \text{ K}^{-1}$. The TEC values of $\text{Sr}_2\text{Fe}_{1.2}\text{Mg}_{0.2}\text{Mo}_{0.6}\text{O}_{6-\delta}$ and $\text{Sr}_2\text{Fe}_{0.9}\text{Mg}_{0.4}\text{Mo}_{0.7}\text{O}_{6-\delta}$ are relatively small in the oxidizing and reducing conditions (see Table 2), and those values are very close to the TECs of typical electrolytes, such as: $\text{La}_{0.9}\text{Sr}_{0.1}\text{Ga}_{0.8}\text{Mg}_{0.2}\text{O}_{3-\delta}$ — $12.17 \times 10^{-6} \text{ K}^{-1}$, $\text{Zr}_{0.85}\text{Y}_{0.15}\text{O}_{2-\delta}$ — $10.8 \times 10^{-6} \text{ K}^{-1}$ and $\text{Ce}_{0.8}\text{Gd}_{0.2}\text{O}_{2-\delta}$ — $12.5 \times 10^{-6} \text{ K}^{-1}$ [24]. Therefore, in the case of the application of redox-stable $\text{Sr}_2\text{Fe}_{1.2}\text{Mg}_{0.2}\text{Mo}_{0.6}\text{O}_{6-\delta}$ and $\text{Sr}_2\text{Fe}_{0.9}\text{Mg}_{0.4}\text{Mo}_{0.7}\text{O}_{6-\delta}$ double perovskites as electrode materials for S-SOFCs, the delamination problem is alleviated, possibly providing a stable cell performance.

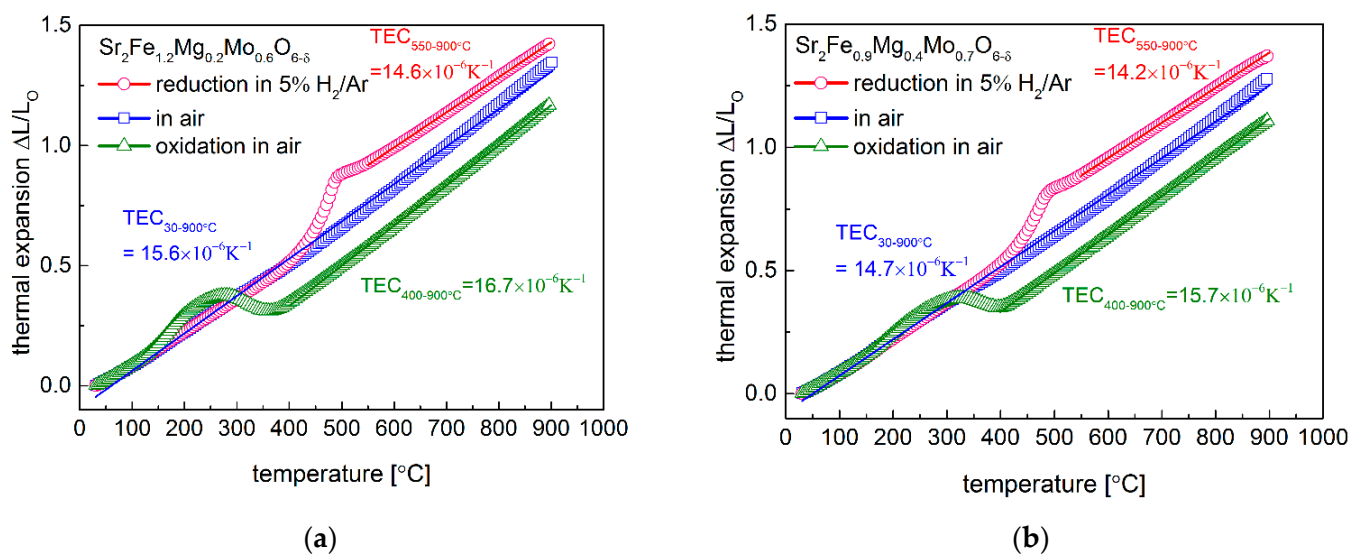


Figure 4. Thermal expansion behavior of (a) $\text{Sr}_2\text{Fe}_{1.2}\text{Mg}_{0.2}\text{Mo}_{0.6}\text{O}_{6-\delta}$ and (b) $\text{Sr}_2\text{Fe}_{0.9}\text{Mg}_{0.4}\text{Mo}_{0.7}\text{O}_{6-\delta}$ materials in air, reduction in 5 vol.% H_2/argon , and oxidation in air of the reduced oxides.

The oxygen content of $\text{Sr}_2\text{Fe}_{1.2}\text{Mg}_{0.2}\text{Mo}_{0.6}\text{O}_{6-\delta}$ and $\text{Sr}_2\text{Fe}_{0.9}\text{Mg}_{0.4}\text{Mo}_{0.7}\text{O}_{6-\delta}$ at room temperature was determined by iodometric titration. $\text{Sr}_2\text{Fe}_{1.2}\text{Mg}_{0.2}\text{Mo}_{0.6}\text{O}_{5.90}$ and $\text{Sr}_2\text{Fe}_{0.9}\text{Mg}_{0.4}\text{Mo}_{0.7}\text{O}_{5.93}$ are obtained at room temperature, which shows the presence of the same average iron oxidation state, with +3.17 in both materials. This indicates the considerable dominant existence of Fe^{3+} (83.3%) and a small amount of Fe^{4+} (16.7%) present in both $\text{Sr}_2\text{Fe}_{1.2}\text{Mg}_{0.2}\text{Mo}_{0.6}\text{O}_{5.90}$ and $\text{Sr}_2\text{Fe}_{0.9}\text{Mg}_{0.4}\text{Mo}_{0.7}\text{O}_{5.93}$ perovskites. The oxygen content change of $\text{Sr}_2\text{Fe}_{1.2}\text{Mg}_{0.2}\text{Mo}_{0.6}\text{O}_{6-\delta}$ and $\text{Sr}_2\text{Fe}_{0.9}\text{Mg}_{0.4}\text{Mo}_{0.7}\text{O}_{6-\delta}$ oxides was measured as a function of temperature up to 900 °C by TG studies in air and in argon, respectively

(Figure 5a,b). The measured oxygen content of materials is presented in Table 3. Both the two samples show a similar content of oxygen nonstoichiometry at 900 °C in air, with $\delta = 0.18$ for $\text{Sr}_2\text{Fe}_{1.2}\text{Mg}_{0.2}\text{Mo}_{0.6}\text{O}_{6-\delta}$ and $\delta = 0.17$ for $\text{Sr}_2\text{Fe}_{0.9}\text{Mg}_{0.4}\text{Mo}_{0.7}\text{O}_{6-\delta}$. The additional oxygen vacancies in the high-temperature range are created in the materials, according to the reaction: $\text{O}_\text{O}^\times \leftrightarrow 1/2\text{O}_2 + \text{V}_\text{O}^{\bullet\bullet} + 2e^-$. In the argon atmosphere, a substantial oxygen content change has been recorded for both the two materials. The initial start of a considerable oxygen content drop is at around 350 °C. Since the reduction energies of $\text{Fe}^{3+}/\text{Fe}^{2+}$ are much lower than that of $\text{Mo}^{6+}/\text{Mo}^{5+}$ [4,28], the first reduction in the samples can be ascribed to the reduction in iron cations to Fe^{2+} . The second step change (above 550 °C) can be related with the reduction in Mo^{6+} to $\text{Mo}^{5+}/\text{Mo}^{4+}$ and the further increase in the oxygen vacancies concentration [28]. The oxygen contents of $\text{Sr}_2\text{Fe}_{1.2}\text{Mg}_{0.2}\text{Mo}_{0.6}\text{O}_{6-\delta}$ and $\text{Sr}_2\text{Fe}_{0.9}\text{Mg}_{0.4}\text{Mo}_{0.7}\text{O}_{6-\delta}$ samples in argon are 5.17 and 5.28, respectively. Therefore, the relative oxygen nonstoichiometry changes $\Delta\delta$ of $\text{Sr}_2\text{Fe}_{1.2}\text{Mg}_{0.2}\text{Mo}_{0.6}\text{O}_{6-\delta}$ and $\text{Sr}_2\text{Fe}_{0.9}\text{Mg}_{0.4}\text{Mo}_{0.7}\text{O}_{6-\delta}$ samples in argon up to 900 °C are 0.73 and 0.65, respectively. The higher content of redox couples of $\text{Fe}^{3+}/\text{Fe}^{2+}$ and $\text{Mo}^{6+}/\text{Mo}^{5+}$ in less Mg-doped $\text{Sr}_2\text{Fe}_{1.2}\text{Mg}_{0.2}\text{Mo}_{0.6}\text{O}_{6-\delta}$ allows for a generation of more oxygen vacancies than in $\text{Sr}_2\text{Fe}_{0.9}\text{Mg}_{0.4}\text{Mo}_{0.7}\text{O}_{6-\delta}$, which indicates that the increased content of magnesium in materials does not favor the creation of oxygen vacancies.

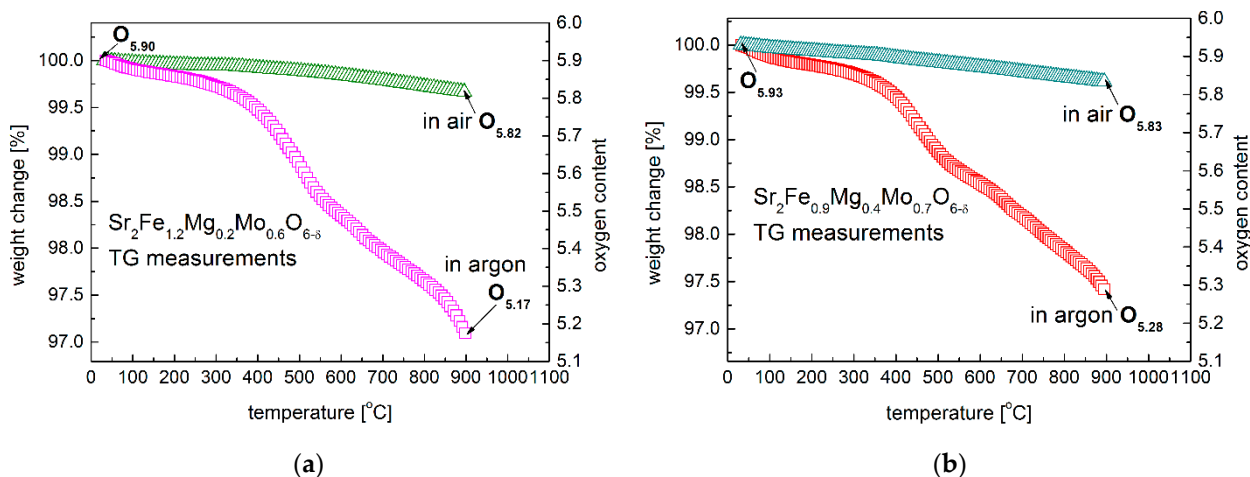


Figure 5. Oxygen content change of (a) $\text{Sr}_2\text{Fe}_{1.2}\text{Mg}_{0.2}\text{Mo}_{0.6}\text{O}_{6-\delta}$ and (b) $\text{Sr}_2\text{Fe}_{0.9}\text{Mg}_{0.4}\text{Mo}_{0.7}\text{O}_{6-\delta}$ oxides in air and argon, respectively.

Table 2. Thermal expansion coefficients TEC [10^{-6} K^{-1}] of $\text{Sr}_2\text{Fe}_{1.2}\text{Mg}_{0.2}\text{Mo}_{0.6}\text{O}_{6-\delta}$ and $\text{Sr}_2\text{Fe}_{0.9}\text{Mg}_{0.4}\text{Mo}_{0.7}\text{O}_{6-\delta}$ oxides from dilatometer measurements and high-temperature XRD studies in air.

	HT-XRD (30–250 °C)	HT-XRD (350–900 °C)	Dilatometer (30–900 °C in Air)	Dilatometer (400–900 °C, Oxidation in Air)	Dilatometer (550–900 °C, Reduction in 5% H_2/Ar)
$\text{Sr}_2\text{Fe}_{1.2}\text{Mg}_{0.2}\text{Mo}_{0.6}\text{O}_{6-\delta}$	12.9	14.6	15.6	16.7	14.6
$\text{Sr}_2\text{Fe}_{0.9}\text{Mg}_{0.4}\text{Mo}_{0.7}\text{O}_{6-\delta}$	15.1	13.5	14.7	15.7	14.2

Table 3. Oxygen content of $\text{Sr}_2\text{Fe}_{1.2}\text{Mg}_{0.2}\text{Mo}_{0.6}\text{O}_{6-\delta}$ and $\text{Sr}_2\text{Fe}_{0.9}\text{Mg}_{0.4}\text{Mo}_{0.7}\text{O}_{6-\delta}$ oxides at 600–900 °C in air and argon.

$\text{Sr}_2\text{Fe}_{1.2}\text{Mg}_{0.2}\text{Mo}_{0.6}\text{O}_{6-\delta}$	600 °C in air	700 °C in air	800 °C in air	900 °C in air
	Oxygen content	5.86	5.85	5.83
$\text{Sr}_2\text{Fe}_{1.2}\text{Mg}_{0.2}\text{Mo}_{0.6}\text{O}_{6-\delta}$	600 °C in argon	700 °C in argon	800 °C in argon	900 °C in argon
	Oxygen content	5.49	5.39	5.31
$\text{Sr}_2\text{Fe}_{0.9}\text{Mg}_{0.4}\text{Mo}_{0.7}\text{O}_{6-\delta}$	600 °C in air	700 °C in air	800 °C in air	900 °C in air
	Oxygen content	5.87	5.86	5.85
$\text{Sr}_2\text{Fe}_{0.9}\text{Mg}_{0.4}\text{Mo}_{0.7}\text{O}_{6-\delta}$	600 °C in argon	700 °C in argon	800 °C in argon	900 °C in argon
	Oxygen content	5.57	5.48	5.39

3.3. The Transport Properties

The electrical conductivity data gathered between 200–900 °C for $\text{Sr}_2\text{Fe}_{1.2}\text{Mg}_{0.2}\text{Mo}_{0.6}\text{O}_{6-\delta}$ and $\text{Sr}_2\text{Fe}_{0.9}\text{Mg}_{0.4}\text{Mo}_{0.7}\text{O}_{6-\delta}$ samples show the increased doping content of magnesium decreases the total conductivity and increases the activation energy in air and 5 vol. H_2/Ar (Figure 6a). In materials, the electrons are transmitted via the $\text{Fe}^{2+}/\text{Fe}^{3+}-\text{O}^{2-}-\text{Fe}^{3+}/\text{Fe}^{4+}$ network. The Mg doping in the samples reduces the content of iron, thus resulting in the decrease in electrical conductivities. For both the two samples, the conductivity measured in air shows a maximum value with temperature: it increases initially and then drops. Samples exhibit a linear relationship in the low-temperature range (<600 °C), indicating small polaron conduction behavior. $\text{Sr}_2\text{Fe}_{1.2}\text{Mg}_{0.2}\text{Mo}_{0.6}\text{O}_{6-\delta}$ ($E_a = 0.09$ eV) possesses a slightly smaller activation energy than that of $\text{Sr}_2\text{Fe}_{0.9}\text{Mg}_{0.4}\text{Mo}_{0.7}\text{O}_{6-\delta}$ ($E_a = 0.10$ eV). In the case of $\text{Sr}_2\text{Fe}_{1.2}\text{Mg}_{0.2}\text{Mo}_{0.6}\text{O}_{6-\delta}$, the maximum conductivity of $56.2 \text{ S}\cdot\text{cm}^{-1}$ was recorded at around 600 °C, while for $\text{Sr}_2\text{Fe}_{0.9}\text{Mg}_{0.4}\text{Mo}_{0.7}\text{O}_{6-\delta}$, the peak value with $8.0 \text{ S}\cdot\text{cm}^{-1}$ was measured at 700 °C. The conductivity decreases with the further increase in the temperature, which can be associated with the release of lattice oxygen ($\text{O}_\text{O}^\times \leftrightarrow 1/2\text{O}_2 + \text{V}_\text{O}^{\bullet\bullet} + 2e^-$) at high temperatures breaking the $\text{Fe}^{3+}-\text{O}^{2-}-\text{Fe}^{4+}$ network, resulting in the decrease in electrical conductivities. Similar phenomena have been recorded in other SrFeO_3 -based materials [28,41]. In the reducing atmosphere (5 vol.% H_2/Ar), both $\text{Sr}_2\text{Fe}_{1.2}\text{Mg}_{0.2}\text{Mo}_{0.6}\text{O}_{6-\delta}$ and $\text{Sr}_2\text{Fe}_{0.9}\text{Mg}_{0.4}\text{Mo}_{0.7}\text{O}_{6-\delta}$ compounds show much lower conductivity. The $\text{Sr}_2\text{Fe}_{1.2}\text{Mg}_{0.2}\text{Mo}_{0.6}\text{O}_{6-\delta}$ sample possesses a relatively satisfactory conductivity value ($10.3 \text{ S}\cdot\text{cm}^{-1}$ at 800 °C) with a very small activation energy $E_a = 0.04$ eV. The $\text{Sr}_2\text{Fe}_{1.2}\text{Mg}_{0.2}\text{Mo}_{0.6}\text{O}_{6-\delta}$ material shows much higher conductivity in air and comparable values in the reducing condition with $\text{Sr}_2\text{FeMo}_{2/3}\text{Mg}_{1/3}\text{O}_{6-\delta}$ oxide ($4\text{--}5 \text{ S}\cdot\text{cm}^{-1}$ in air, and $9\text{--}13 \text{ S}\cdot\text{cm}^{-1}$ in H_2 at 600–800 °C) [38]. In addition, the measured electrical conductivity of $\text{Sr}_2\text{Fe}_{1.2}\text{Mg}_{0.2}\text{Mo}_{0.6}\text{O}_{6-\delta}$ is much higher than the σ value of $\text{Sr}_2\text{MgMoO}_{6-\delta}$ [49], $\text{Sr}_2\text{Fe}_{1.5}\text{Mo}_{0.3}\text{Cu}_{0.2}\text{O}_{6-\delta}$ [35], $\text{Sr}_{2-x}\text{Ba}_x\text{MgMoO}_{6-\delta}$, and $\text{Sr}_{2-x}\text{Ba}_x\text{MnMoO}_{6-\delta}$ [24,25]. In addition, the chemical diffusion coefficient D and surface exchange constant k of $\text{Sr}_2\text{Fe}_{1.2}\text{Mg}_{0.2}\text{Mo}_{0.6}\text{O}_{6-\delta}$ have been determined by the mass relaxation technique (Figure 6b,c). The D coefficient is in the range of 6.3×10^{-6} to $6.3 \times 10^{-5} \text{ cm}^2 \text{ s}^{-1}$ at 600–800 °C, with the activation energy $E_{a,D} = 0.96$ eV. The k constant is within the scope of 2.0×10^{-4} – $5.6 \times 10^{-4} \text{ cm s}^{-1}$, with the activation energy $E_{a,k} = 0.396$ eV. The measured chemical diffusion coefficients D are comparable with the D recorded for $\text{Sr}_2\text{TiNi}_{0.5}\text{Mo}_{0.5}\text{O}_{6-\delta}$ [37] and $\text{Sr}_2\text{Fe}_{1.4}\text{Mn}_{0.1}\text{Mo}_{0.5}\text{O}_{6-\delta}$ [50] materials, while the k values of $\text{Sr}_2\text{Fe}_{1.2}\text{Mg}_{0.2}\text{Mo}_{0.6}\text{O}_{6-\delta}$ are slightly smaller than k of $\text{Sr}_2\text{Fe}_{1.4}\text{Mn}_{0.1}\text{Mo}_{0.5}\text{O}_{6-\delta}$ [50]. The relatively high diffusion coefficients D and k measured for $\text{Sr}_2\text{Fe}_{1.2}\text{Mg}_{0.2}\text{Mo}_{0.6}\text{O}_{6-\delta}$ oxide indicate the good ionic transport in such a material.

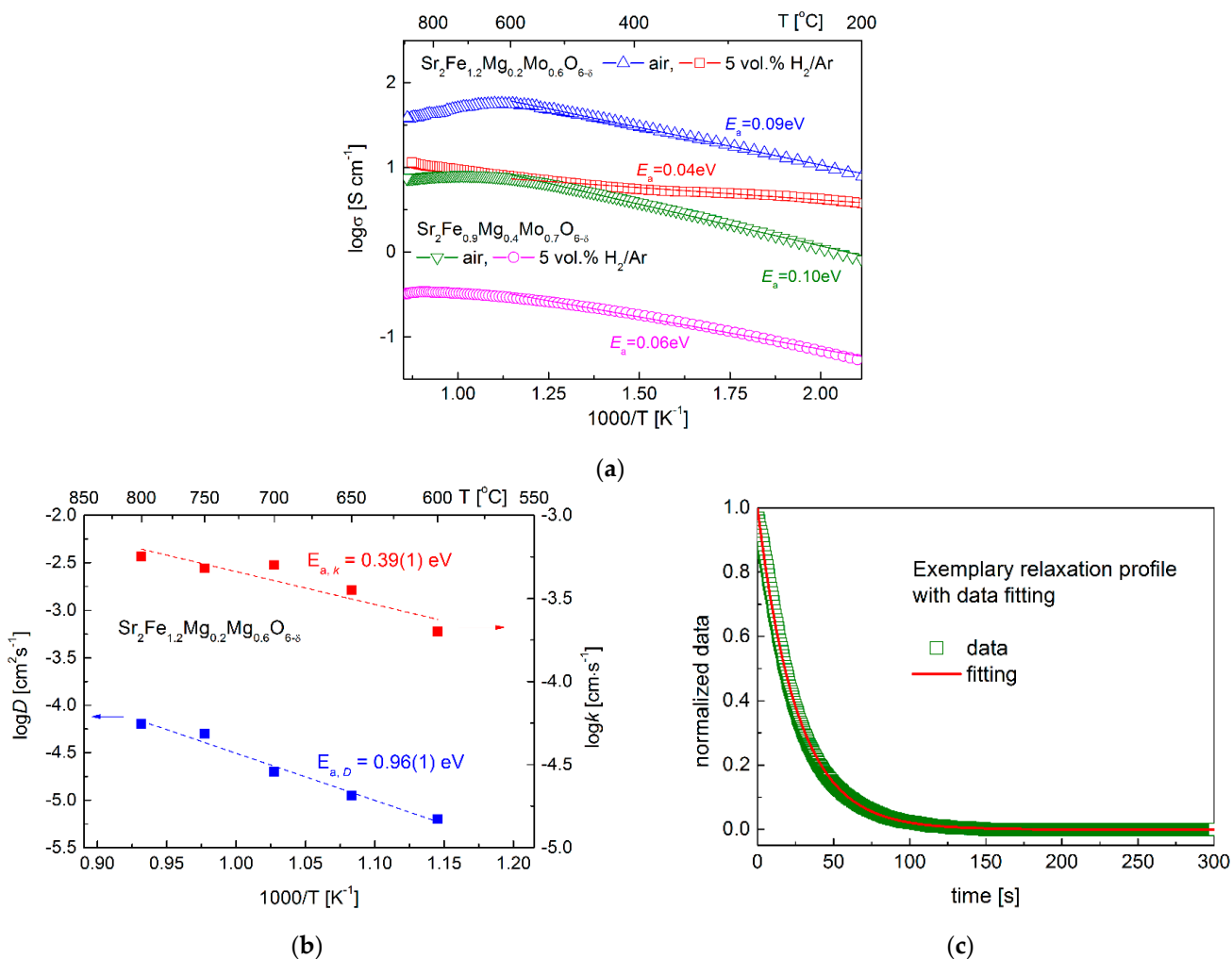


Figure 6. (a) Electrical conductivity of $\text{Sr}_2\text{Fe}_{1.2}\text{Mg}_{0.2}\text{Mo}_{0.6}\text{O}_{6-\delta}$ and $\text{Sr}_2\text{Fe}_{0.9}\text{Mg}_{0.4}\text{Mo}_{0.7}\text{O}_{6-\delta}$ materials in air and 5 vol.% H₂/Ar, (b) diffusion coefficients D and k measured as a function of temperature for $\text{Sr}_2\text{Fe}_{1.2}\text{Mg}_{0.2}\text{Mo}_{0.6}\text{O}_{6-\delta}$ sample, and (c) an exemplary normalized relaxation profile with fitting.

The ionic conductivity σ_i of $\text{Sr}_2\text{Fe}_{1.2}\text{Mg}_{0.2}\text{Mo}_{0.6}\text{O}_{6-\delta}$ oxide was also evaluated using the Nernst–Einstein equation: $\sigma_i = \frac{c_O \cdot q^2 D_s}{RT} = \frac{2c_O \cdot q^2 D \cdot d \ln c_O}{RT \cdot d \ln p_{\text{O}_2}}$, where: c_O —concentration of oxygen, q —charge of mole of oxygen anions, D_s —self-diffusion coefficient, R —gas constant, T —temperature [51]. The ionic conductivity σ_i of $\text{Sr}_2\text{Fe}_{1.2}\text{Mg}_{0.2}\text{Mo}_{0.6}\text{O}_{6-\delta}$ oxide was estimated to be about 0.005 S·cm⁻¹ at 800 °C. For the calculation, the high-temperature XRD-based density of the sample recorded at 800 °C was used, together with the determined oxygen content, allowing the obtaining of the c_O value. In the calculation, all oxygen anions were considered as participating in the ionic transport, which may be a factor generating the biggest error for the performed evaluation. Despite the mentioned error source, the evaluated ionic conductivity σ_i of $\text{Sr}_2\text{Fe}_{1.2}\text{Mg}_{0.2}\text{Mo}_{0.6}\text{O}_{6-\delta}$ is reasonable and comparable with the measured σ_i values for $\text{Sr}_2\text{Mg}_{1-x}\text{Co}_x\text{MoO}_{6-\delta}$ ($x = 0, 0.3$ and 0.7) samples at 800 °C [40]. Therefore, compared with the most crucial physicochemical proprieties of $\text{Sr}_2(\text{Fe},\text{Mo})\text{O}_{6-\delta}$ -type materials presented in the Table 4, $\text{Sr}_2\text{Fe}_{1.2}\text{Mg}_{0.2}\text{Mo}_{0.6}\text{O}_{6-\delta}$ oxide can potentially be a good electrode material candidate for S-SOFCs.

Table 4. The structural properties, electrical conductivity, TEC values, and redox stability of Sr₂(Fe,Mo)O_{6-δ}-type materials.

Compound	Crystal Structure	Electrical Conductivity [S·cm ⁻¹]	TEC [×10 ⁻⁶ K ⁻¹]	Redox Stability	References
Sr ₂ Fe _{1.2} Mg _{0.2} Mo _{0.6} O _{6-δ}	<i>Fm-3m</i>	56.23–42.66 in air 600–800 °C; 7.88–10.26 in 5% H ₂ /Ar 600–800 °C	12.9–14.6 in air; 14.6–16.7 in 5% H ₂ /Ar	redox stable	This work
Sr ₂ Fe _{0.9} Mg _{0.4} Mo _{0.7} O _{6-δ}	<i>Fm-3m</i>	7.90–7.48 in air 600–800 °C; 0.29–0.34 in 5% H ₂ /Ar 600–800 °C	13.5–15.7 in air; 14.2–15.1 in 5% H ₂ /Ar	redox stable	This work
Sr ₂ Fe _{1.5} Mo _{0.3} Cu _{0.2} O _{6-δ}	<i>Fm-3m</i>	0.06–0.36 in 5% H ₂ /Ar at 600–850 °C	-	decomposed in H ₂	[35]
Sr ₂ Fe _{1.5} Mo _{0.5} O _{6-δ}	<i>Fm-3m</i>	2.89–5.55 in 5% H ₂ /Ar at 600–850 °C	-	Redox stable	[35]
	<i>Pm-3m</i>	13 in air at 400–600 °C 50 in 5% H ₂ /Ar at 850 °C	13.5–18.3 in air	Redox stable	[28]
SrFe _{0.5} Mn _{0.25} Mo _{0.25} O _{3-δ}	<i>Pm-3m</i>	3 in air at 850 °C 10 in 5% H ₂ /Ar at 850 °C	12.9–14.5 in air	Redox stable	[28]
Sr ₂ MgMoO _{6-δ}	<i>I-1</i>	0.8 @800 °C in 5% H ₂ /Ar; 0.003 in air @800 °C	-	stable up to 1200 °C in 5% H ₂ /Ar	[49]
La _{0.5} Sr _{0.5} Fe _{0.9} Mo _{0.1} O _{3-δ}	<i>Pm-3m</i>	2.7–6.7 in H ₂ , 600–800 °C	13.4 in air; 15.1 in 5% H ₂ /Ar	stable up to 750 °C in H ₂	[52]
Sr _{1.9} Fe _{1.5} Mo _{0.3} Cu _{0.2} O _{6-δ}	-	54.8 in air 630 °C	19.39 in air	decomposed in H ₂	[53]
Sr ₂ FeMo _{2/3} Mg _{1/3} O _{6-δ}	<i>Fm-3m</i>	4–5 in air 600–800 °C; 9–13 in H ₂ 600–800 °C	16.9 in air	Redox stable	[38]
Sr ₂ Fe _{1.3} Ti _{0.1} Mo _{0.6} O _{6-δ}	<i>Fm-3m</i>	220–160 in 5% H ₂ /Ar at 500–800 °C	13.5 in air to 550 °C	Stable in H ₂	[36]
Sr ₂ TiFe _{0.5} Mo _{0.5} O _{6-δ}	<i>Pm-3m</i>	22.3 in H ₂ at 800 °C	11.2 in H ₂	stable in H ₂ and syngas fuels	[54]
Sr ₂ Mg _{0.95} Al _{0.05} MoO _{6-δ}	-	5.4 in 5% H ₂ /Ar at 800 °C	-	Redox stable	[55]
Sr ₂ TiNi _{0.5} Mo _{0.5} O _{6-δ}	-	17.5 in H ₂ at 800 °C	12.8 in air	stable in humidified H ₂	[37]
Sr _{2-x} Ba _x FeMoO _{6-δ}	<i>I4/m</i> (x = 0); <i>Fm-3m</i> (others)	100–1000 in 5% H ₂ /Ar	13.8 in air (for x = 0)	Stable in 5% H ₂ /Ar	[24,25]
Sr _{2-x} Ba _x MnMoO _{6-δ}	<i>P2₁/n</i> (x = 0); <i>Fm-3m</i> (others)	0.24–1.41 in 5% H ₂ /Ar	11.5–14.8 in air (for x = 0)	Stable in 5% H ₂ /Ar	[24,25]
Sr _{2-x} Ba _x MgMoO _{6-δ}	<i>I4/m</i> (x = 0); <i>Fm-3m</i> (others)	0.14–1.38 in 5% H ₂ /Ar	13.8–18.2 in air (for x = 0)	Redox stable	[24,25]
Sr ₂ Mg _{0.3} Co _{0.7} MoO _{6-δ}	<i>I-1</i>	9–7 in 5% H ₂ /Ar at 600–800 °C	13.9 in air	-	[40]
SrFe _{0.45} Co _{0.45} Mo _{0.1} O _{3-δ}	<i>Pm-3m</i>	298 in air at 300 °C	14.8–30.8 in air	Stable in air	[39]

3.4. Chemical Stability and Compatibility of Electrode Materials with Electrolytes

The chemical stability of electrode materials and their compatibility with the used electrolytes in an operating temperature range are critical for the long and stable performance of SOFCs. Therefore, the chemical stability and compatibility of $\text{Sr}_2\text{Fe}_{1.2}\text{Mg}_{0.2}\text{Mo}_{0.6}\text{O}_{6-\delta}$ and $\text{Sr}_2\text{Fe}_{0.9}\text{Mg}_{0.4}\text{Mo}_{0.7}\text{O}_{6-\delta}$ with typical electrolytes $\text{Ce}_{0.8}\text{Gd}_{0.2}\text{O}_{1.9}$ (CGO20) and $\text{La}_{0.8}\text{Sr}_{0.2}\text{Ga}_{0.8}\text{Mg}_{0.2}\text{O}_{3-\delta}$ (LSGM) have been investigated at 1200 °C for 4 h in air. The Rietveld-refined XRD patterns of $\text{Sr}_2\text{Fe}_{1.2}\text{Mg}_{0.2}\text{Mo}_{0.6}\text{O}_{6-\delta}$ and $\text{Sr}_2\text{Fe}_{0.9}\text{Mg}_{0.4}\text{Mo}_{0.7}\text{O}_{6-\delta}$ with electrolyte (50:50 wt.%) powder mixtures are presented in Figure 7a–d. In Figure 7a,b, the XRD data after the studies of electrode materials with CGO20 show no additional phase, confirming the good chemical stability and compatibility of the electrode materials with the $\text{Ce}_{0.8}\text{Gd}_{0.2}\text{O}_{1.9}$ electrolyte. Moreover, as can be observed from Table 5, the refined unit cell parameters of $\text{Sr}_2\text{Fe}_{1.2}\text{Mg}_{0.2}\text{Mo}_{0.6}\text{O}_{6-\delta}$ and $\text{Sr}_2\text{Fe}_{0.9}\text{Mg}_{0.4}\text{Mo}_{0.7}\text{O}_{6-\delta}$ after the chemical stability and compatibility studies are slightly smaller but very close to the results of as-synthesized materials presented in Table 1. The smaller unit cell parameters recorded after the annealing at 1200 °C for 4 h in air indicates the increased content of present Fe^{4+} (high oxygen state) in the materials. The studies show the possible long stable operation of SOFCs with $\text{Sr}_2\text{Fe}_{1.2}\text{Mg}_{0.2}\text{Mo}_{0.6}\text{O}_{6-\delta}$ and $\text{Sr}_2\text{Fe}_{0.9}\text{Mg}_{0.4}\text{Mo}_{0.7}\text{O}_{6-\delta}$ electrode materials towards the typical electrolyte $\text{Ce}_{0.8}\text{Gd}_{0.2}\text{O}_{1.9}$. However, the studies on $\text{Sr}_2\text{Fe}_{1.2}\text{Mg}_{0.2}\text{Mo}_{0.6}\text{O}_{6-\delta}$ and $\text{Sr}_2\text{Fe}_{0.9}\text{Mg}_{0.4}\text{Mo}_{0.7}\text{O}_{6-\delta}$ with $\text{La}_{0.8}\text{Sr}_{0.2}\text{Ga}_{0.8}\text{Mg}_{0.2}\text{O}_{3-\delta}$ show the incompatibility of electrode materials with LSGM electrolyte, with the appearance of additional impurities observed in Figure 7c,d.

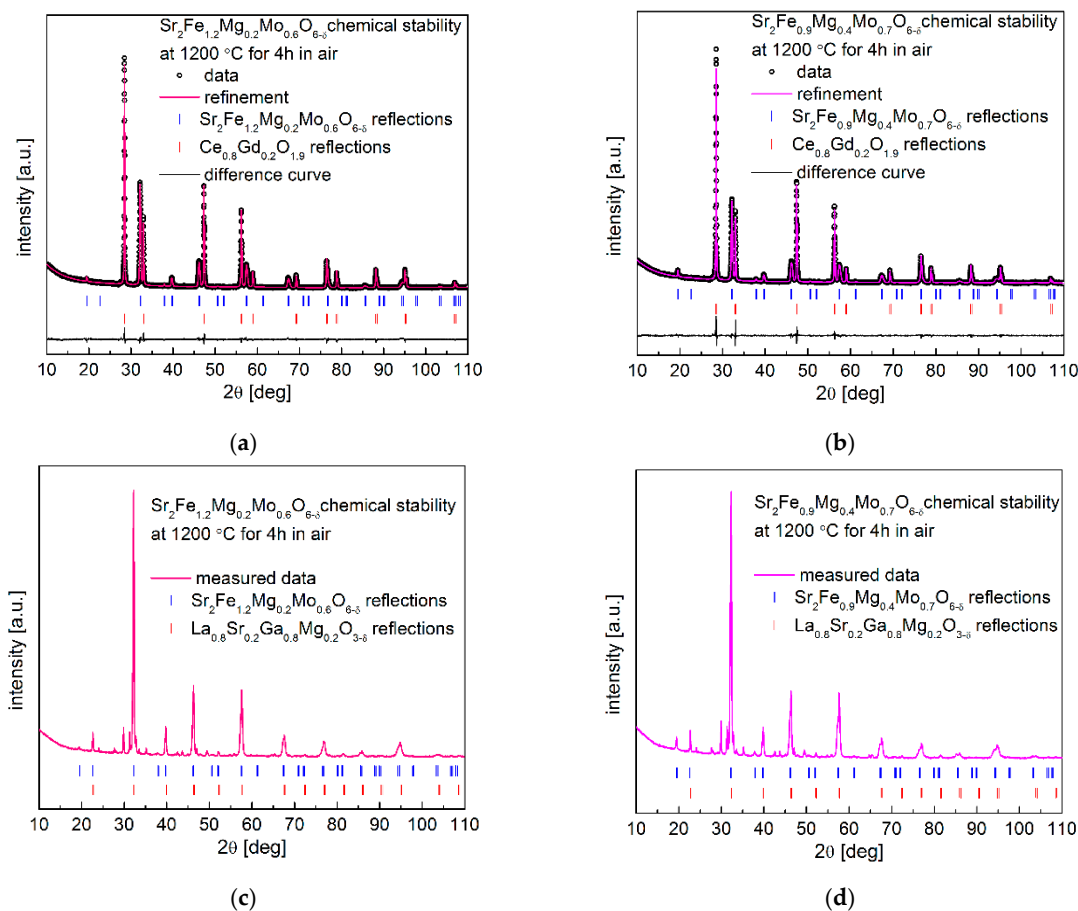


Figure 7. XRD patterns recorded for (a) $\text{Sr}_2\text{Fe}_{1.2}\text{Mg}_{0.2}\text{Mo}_{0.6}\text{O}_{6-\delta}$ and (b) $\text{Sr}_2\text{Fe}_{0.9}\text{Mg}_{0.4}\text{Mo}_{0.7}\text{O}_{6-\delta}$ with CGO20 electrolyte, (c) $\text{Sr}_2\text{Fe}_{1.2}\text{Mg}_{0.2}\text{Mo}_{0.6}\text{O}_{6-\delta}$, and (d) $\text{Sr}_2\text{Fe}_{0.9}\text{Mg}_{0.4}\text{Mo}_{0.7}\text{O}_{6-\delta}$ with LSGM electrolyte, after sintering at 1200 °C for 4 h in air.

Table 5. Structural parameters of $\text{Sr}_2\text{Fe}_{1.2}\text{Mg}_{0.2}\text{Mo}_{0.6}\text{O}_{6-\delta}$ and $\text{Sr}_2\text{Fe}_{0.9}\text{Mg}_{0.4}\text{Mo}_{0.7}\text{O}_{6-\delta}$ oxides with $\text{Ce}_{0.8}\text{Gd}_{0.2}\text{O}_{1.9}$ from 50:50 wt.% mixtures annealed in air for 4 h at 1200 °C.

Composition	$\text{Sr}_2\text{Fe}_{1.2}\text{Mg}_{0.2}\text{Mo}_{0.6}\text{O}_{6-\delta}$	$\text{Ce}_{0.8}\text{Gd}_{0.2}\text{O}_{1.9}$	$\text{Sr}_2\text{Fe}_{0.9}\text{Mg}_{0.4}\text{Mo}_{0.7}\text{O}_{6-\delta}$	$\text{Ce}_{0.8}\text{Gd}_{0.2}\text{O}_{1.9}$
space group	<i>Fm-3m</i>	<i>Fm-3m</i>	<i>Fm-3m</i>	<i>Fm-3m</i>
<i>a</i> [Å]	7.8567(1)	5.4249(1)	7.8657(1)	5.4256(1)
<i>V</i> [Å ³]	484.98(1)	159.66(1)	486.64(1)	159.71(1)
<i>R_p</i> (%)		1.82		2.16
<i>R_{wp}</i> (%)		2.55		3.29

In addition, the long-term chemical compatibility of the $\text{Sr}_2\text{Fe}_{1.2}\text{Mg}_{0.2}\text{Mo}_{0.6}\text{O}_{6-\delta}$ and $\text{Sr}_2\text{Fe}_{0.9}\text{Mg}_{0.4}\text{Mo}_{0.7}\text{O}_{6-\delta}$ electrode materials with $\text{Ce}_{0.8}\text{Gd}_{0.2}\text{O}_{1.9}$ was investigated in 5 vol.% H_2 in argon at 800 °C for 100 h. The collected XRD data after such studies shown in Figure 8a,b also confirm the excellent chemical stability and compatibility of the proposed electrode materials with the $\text{Ce}_{0.8}\text{Gd}_{0.2}\text{O}_{1.9}$ electrolyte. Interestingly, as expected, the unit cell parameters of $\text{Sr}_2\text{Fe}_{1.2}\text{Mg}_{0.2}\text{Mo}_{0.6}\text{O}_{6-\delta}$ and $\text{Sr}_2\text{Fe}_{0.9}\text{Mg}_{0.4}\text{Mo}_{0.7}\text{O}_{6-\delta}$ after the long-term reduction at 800 °C (Table 6) are smaller than the values of materials reduced at 1000 °C (See Table 1). This is related to the lower content of reduced iron and molybdenum cations (contributing to smaller unit cell parameters) in materials annealed at 800 °C in 5 vol.% H_2/Ar . The unit cell parameters of $\text{Ce}_{0.8}\text{Gd}_{0.2}\text{O}_{1.9}$ presented in Table 6 are very close but a little bit bigger than the values of $\text{Ce}_{0.8}\text{Gd}_{0.2}\text{O}_{1.9}$ recorded in Table 5, indicating the stability of $\text{Ce}_{0.8}\text{Gd}_{0.2}\text{O}_{1.9}$ in the presence of studied electrode materials and a slight reduction in $\text{Ce}_{0.8}\text{Gd}_{0.2}\text{O}_{1.9}$ in the atmosphere of 5 vol.% H_2/Ar .

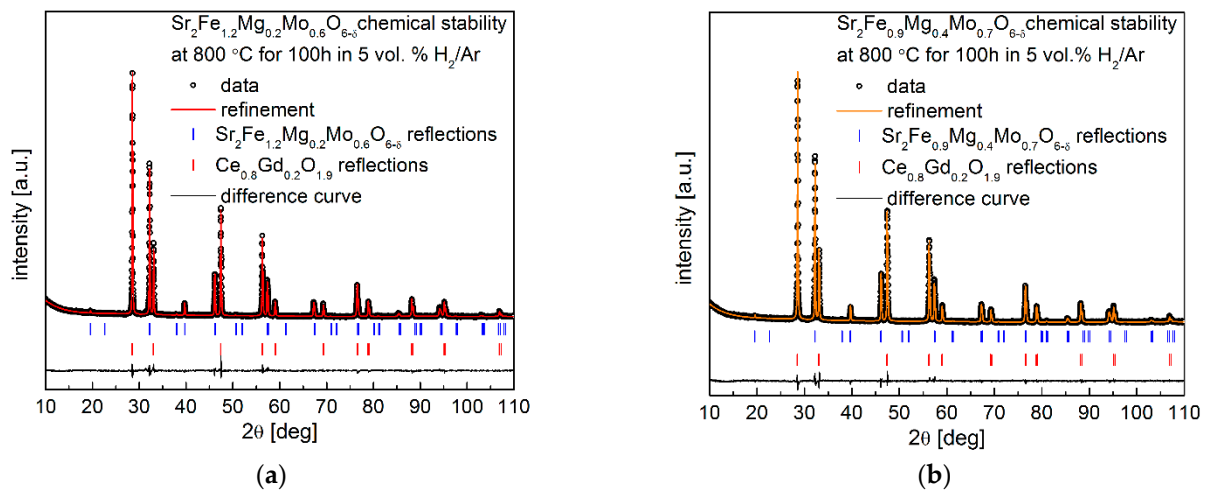


Figure 8. XRD patterns recorded for (a) $\text{Sr}_2\text{Fe}_{1.2}\text{Mg}_{0.2}\text{Mo}_{0.6}\text{O}_{6-\delta}$ and (b) $\text{Sr}_2\text{Fe}_{0.9}\text{Mg}_{0.4}\text{Mo}_{0.7}\text{O}_{6-\delta}$ with the $\text{Ce}_{0.8}\text{Gd}_{0.2}\text{O}_{1.9}$ electrolyte after annealing in 5 vol.% H_2/Ar at 800 °C for 100 h.

Table 6. Structural parameters of $\text{Sr}_2\text{Fe}_{1.2}\text{Mg}_{0.2}\text{Mo}_{0.6}\text{O}_{6-\delta}$ and $\text{Sr}_2\text{Fe}_{0.9}\text{Mg}_{0.4}\text{Mo}_{0.7}\text{O}_{6-\delta}$ oxides with $\text{Ce}_{0.8}\text{Gd}_{0.2}\text{O}_{1.9}$ from 50:50 wt.% mixtures annealed in 5 vol.% H_2/Ar at 800 °C for 100 h.

Composition	$\text{Sr}_2\text{Fe}_{1.2}\text{Mg}_{0.2}\text{Mo}_{0.6}\text{O}_{6-\delta}$	$\text{Ce}_{0.8}\text{Gd}_{0.2}\text{O}_{1.9}$	$\text{Sr}_2\text{Fe}_{0.9}\text{Mg}_{0.4}\text{Mo}_{0.7}\text{O}_{6-\delta}$	$\text{Ce}_{0.8}\text{Gd}_{0.2}\text{O}_{1.9}$
space group	<i>Fm-3m</i>	<i>Fm-3m</i>	<i>Fm-3m</i>	<i>Fm-3m</i>
<i>a</i> [Å]	7.8811(1)	5.4285(1)	7.8801(1)	5.4289(1)
<i>V</i> [Å ³]	489.52(1)	159.97(1)	489.32(1)	160.00(1)
<i>R_p</i> (%)		2.05		1.99
<i>R_{wp}</i> (%)		2.87		2.76

4. Conclusions

The physicochemical properties including the crystal structure properties, redox stability, thermal expansion properties in oxidizing and reducing conditions, oxygen nonstoichiometry as a function of temperature and transport properties, as well as the chemical compatibility with typical electrolytes have been systematically studied for magnesium-doped $\text{Sr}_2\text{Fe}_{1.2}\text{Mg}_{0.2}\text{Mo}_{0.6}\text{O}_{6-\delta}$ and $\text{Sr}_2\text{Fe}_{0.9}\text{Mg}_{0.4}\text{Mo}_{0.7}\text{O}_{6-\delta}$ oxides. $\text{Sr}_2\text{Fe}_{1.2}\text{Mg}_{0.2}\text{Mo}_{0.6}\text{O}_{6-\delta}$ and $\text{Sr}_2\text{Fe}_{0.9}\text{Mg}_{0.4}\text{Mo}_{0.7}\text{O}_{6-\delta}$ compounds crystallize in $Fm-3m$ space group with a double perovskite structure, which is stable in reducing and oxidizing conditions and up to a high-temperature range. The relative volume change between reduced and oxidized materials is very small (especially for $\text{Sr}_2\text{Fe}_{0.9}\text{Mg}_{0.4}\text{Mo}_{0.7}\text{O}_{6-\delta}$, $\Delta V = 0.55\%$), which favors the application of such a material both in reducing and oxidizing conditions. The in situ reduction and oxidation of sinters with dilatometer measurements prove the excellent redox stability of investigated materials in reducing and oxidizing conditions, with TEC values measured very close to the most used solid electrolytes. Mg doping in materials suppresses the thermal expansion of samples in oxidizing and reducing atmospheres. Both materials show a presence of oxygen vacancies, and the oxygen content was determined at room temperature ($\text{Sr}_2\text{Fe}_{1.2}\text{Mg}_{0.2}\text{Mo}_{0.6}\text{O}_{5.90}$ and $\text{Sr}_2\text{Fe}_{0.9}\text{Mg}_{0.4}\text{Mo}_{0.7}\text{O}_{5.93}$) and recorded up to a high temperature range (up to $900\text{ }^\circ\text{C}$), while the increase in magnesium content in materials decreased the oxygen nonstoichiometry δ . $\text{Sr}_2\text{Fe}_{1.2}\text{Mg}_{0.2}\text{Mo}_{0.6}\text{O}_{6-\delta}$ perovskite presents relatively good electrical conductivity in air ($56.2\text{ S}\cdot\text{cm}^{-1}$ at $600\text{ }^\circ\text{C}$) and 5 vol.% H_2/Ar ($10.3\text{ S}\cdot\text{cm}^{-1}$ at $800\text{ }^\circ\text{C}$). The measured relatively high chemical diffusion coefficient D and surface exchange constant k indicates the good ionic conductivity of the material. In addition, the ionic conductivity was also calculated with the value of $0.005\text{ S}\cdot\text{cm}^{-1}$ at $800\text{ }^\circ\text{C}$. The stability studies show that both compounds are compatible with $\text{Ce}_{0.8}\text{Gd}_{0.2}\text{O}_{1.9}$ but react with the $\text{La}_{0.8}\text{Sr}_{0.2}\text{Ga}_{0.8}\text{Mg}_{0.2}\text{O}_{3-d}$ electrolyte. Therefore, the magnesium-doped $\text{Sr}_2\text{Fe}_{1.2}\text{Mg}_{0.2}\text{Mo}_{0.6}\text{O}_{6-\delta}$ double perovskite with excellent redox stability can be potentially applied as stable electrode materials for symmetrical SOFCs and are of great interest for further investigations.

Author Contributions: Conceptualization, methodology, investigation, validation, formal analysis, resources, data curation, writing—original draft preparation, funding acquisition, supervision, K.Z.; visualization, investigation, J.L.; writing—review and editing, H.Z., X.H. and K.Q. All authors have read and agreed to the published version of the manuscript.

Funding: This research was funded by National Science Centre Poland (NCN) on the basis of the decision number UMO-2021/43/D/ST5/00824.

Institutional Review Board Statement: Not applicable.

Informed Consent Statement: Not applicable.

Data Availability Statement: The data presented in this study are available on request from the corresponding author.

Conflicts of Interest: The authors declare no conflict of interest.

References

1. Myung, J.-H.; Neagu, D.; Miller, D.N.; Irvine, J. Switching on electrocatalytic activity in solid oxide cells. *Nature* **2016**, *537*, 528–531. [[CrossRef](#)] [[PubMed](#)]
2. Irvine, J.T.S.; Neagu, D.; Verbraeken, M.C.; Chatzichristodoulou, C.; Graves, C.R.; Mogensen, M.B. Evolution of the electrochemical interface in high-temperature fuel cells and electrolyzers. *Nat. Energy* **2016**, *1*, 15014. [[CrossRef](#)]
3. Park, S.; Vohs, J.M.; Gorte, R.J. Direct oxidation of hydrocarbons in a solid-oxide fuel cell. *Nature* **2000**, *404*, 265–267. [[CrossRef](#)]
4. Huang, Y.-H.; Dass, R.I.; Xing, Z.-L.; Goodenough, J.B.; Goldman, A.S.; Roy, A.H.; Ahuja, R.; Schinski, W.; Brookhart, M. Double Perovskites as Anode Materials for Solid-Oxide Fuel Cells. *Science* **2006**, *312*, 254–257. [[CrossRef](#)]
5. Graves, C.R.; Ebbesen, S.D.; Jensen, S.H.; Simonsen, S.B.; Mogensen, M.B. Eliminating degradation in solid oxide electrochemical cells by reversible operation. *Nat. Mater.* **2015**, *14*, 239–244. [[CrossRef](#)] [[PubMed](#)]
6. Tao, S.; Irvine, J. A redox-stable efficient anode for solid-oxide fuel cells. *Nat. Mater.* **2003**, *2*, 320–323. [[CrossRef](#)]

7. Laguna-Bercero, M.A. Recent advances in high temperature electrolysis using solid oxide fuel cells: A review. *J. Power Sources* **2012**, *203*, 4–16. [[CrossRef](#)]
8. Hughes, G.A.; Railsback, J.G.; Yakal-Kremiski, K.J.; Butts, D.M.; Barnett, S.A. Degradation of $(\text{La}_{0.8}\text{Sr}_{0.2})_{0.98}\text{MnO}_{3-\delta}-\text{Zr}_{0.84}\text{Y}_{0.16}\text{O}_{2-\gamma}$ composite electrodes during reversing current operation. *Faraday Discuss.* **2015**, *182*, 365–377. [[CrossRef](#)]
9. Badding, M.; Brown, J.; Ketcham, T.; Julien, D.S. Solid Oxide Fuel Cells with Symmetric Composite Electrodes. U.S. Patent 20010044043, 15 May 2001. Available online: <https://patents.justia.com/patent/20010044043#description> (accessed on 1 January 2020).
10. Bastidas, D.M.; Tao, S.; Irvine, J.T.S. A symmetrical solid oxide fuel cell demonstrating redox stable perovskite electrodes. *J. Mater. Chem.* **2006**, *16*, 1603–1605. [[CrossRef](#)]
11. Ruiz-Morales, J.C.; Canales-Vázquez, J.; Peña-Martínez, J.; Marrero-López, D.; Núñez, P. On the simultaneous use of $\text{La}_{0.75}\text{Sr}_{0.25}\text{Cr}_{0.5}\text{Mn}_{0.5}\text{O}_{3-\delta}$ as both anode and cathode material with improved microstructure in solid oxide fuel cells. *Electrochim. Acta* **2006**, *52*, 278–284. [[CrossRef](#)]
12. Cable, T.L.; Setlock, J.A.; Farmer, S.C.; Eckel, A.J. Regenerative Performance of the NASA Symmetrical Solid Oxide Fuel Cell Design. *Int. J. Appl. Ceram. Technol.* **2011**, *8*, 1–12. [[CrossRef](#)]
13. Su, C.; Wang, W.; Liu, M.; Tade, M.; Shao, Z. Progress and Prospects in Symmetrical Solid Oxide Fuel Cells with Two Identical Electrodes. *Adv. Energy Mater.* **2015**, *5*, 1500188. [[CrossRef](#)]
14. Sengodan, S.; Choi, S.; Jun, A.; Shin, T.H.; Ju, Y.-W.; Jeong, H.Y.; Shin, J.; Irvine, J.; Kim, G. Layered oxygen-deficient double perovskite as an efficient and stable anode for direct hydrocarbon solid oxide fuel cells. *Nat. Mater.* **2015**, *14*, 205–209. [[CrossRef](#)]
15. Zamudio-García, J.; Caizán-Juanarena, L.; Porrás-Vázquez, J.M.; Losilla, E.R.; Marrero-López, D. A review on recent advances and trends in symmetrical electrodes for solid oxide cells. *J. Power Sources* **2022**, *520*, 230852. [[CrossRef](#)]
16. Zhu, K.; Luo, B.; Liu, Z.; Wen, X. Recent advances and prospects of symmetrical solid oxide fuel cells. *Ceram. Int.* **2022**, *48*, 8972–8986. [[CrossRef](#)]
17. Ding, H.; Fang, S.; Yang, Y.; Yang, Y.; Wu, W.; Tao, Z. High-performing and stable electricity generation by ceramic fuel cells operating in dry methane over 1000 hours. *J. Power Sources* **2018**, *401*, 322–328. [[CrossRef](#)]
18. Ding, H.; Tao, Z.; Liu, S.; Zhang, J. A High-Performing Sulfur-Tolerant and Redox-Stable Layered Perovskite Anode for Direct Hydrocarbon Solid Oxide Fuel Cells. *Sci. Rep.* **2015**, *5*, 18129. [[CrossRef](#)]
19. Zhang, B.; Wan, Y.; Hua, Z.; Tang, K.; Xia, C. Tungsten-Doped $\text{PrBaFe}_2\text{O}_{5+\delta}$ Double Perovskite as a High-Performance Electrode Material for Symmetrical Solid Oxide Fuel Cells. *ACS Appl. Energy Mater.* **2021**, *4*, 8401–8409. [[CrossRef](#)]
20. Xiao, G.; Liu, Q.; Zhao, F.; Zhang, L.; Xia, C.; Chen, F. $\text{Sr}_2\text{Fe}_{1.5}\text{Mo}_{0.5}\text{O}_6$ as Cathodes for Intermediate-Temperature Solid Oxide Fuel Cells with $\text{La}_{0.8}\text{Sr}_{0.2}\text{Ga}_{0.87}\text{Mg}_{0.13}\text{O}_3$ Electrolyte. *J. Electrochem. Soc.* **2011**, *158*, B455. [[CrossRef](#)]
21. Huang, Y.-H.; Dass, R.I.; Denyszyn, J.C.; Goodenough, J.B. Synthesis and Characterization of $\text{Sr}_2\text{MgMoO}_{6-\delta}$: An Anode Material for the Solid Oxide Fuel Cell. *J. Electrochem. Soc.* **2006**, *153*, A1266. [[CrossRef](#)]
22. Marrero-López, D.; Peña-Martínez, J.; Ruiz-Morales, J.C.; Gabás, M.; Núñez, P.; Aranda, M.A.G.; Ramos-Barrado, J.R. Redox behaviour, chemical compatibility and electrochemical performance of $\text{Sr}_2\text{MgMoO}_{6-\delta}$ as SOFC anode. *Solid State Ion.* **2010**, *180*, 1672–1682. [[CrossRef](#)]
23. Skutina, L.; Filonova, E.; Medvedev, D.; Maignan, A. Undoped Sr_2MMoO_6 Double Perovskite Molybdates (M = Ni, Mg, Fe) as Promising Anode Materials for Solid Oxide Fuel Cells. *Materials* **2021**, *14*, 1715. [[CrossRef](#)] [[PubMed](#)]
24. Zheng, K.; Świerczek, K. Physicochemical properties of rock salt-type ordered Sr_2MMoO_6 (M = Mg, Mn, Fe, Co, Ni) double perovskites. *J. Eur. Ceram. Soc.* **2014**, *34*, 4273–4284. [[CrossRef](#)]
25. Zheng, K.; Świerczek, K. A- and B-site doping effect on physicochemical properties of $\text{Sr}_{2-x}\text{Ba}_x\text{MMoO}_6$ (M = Mg, Mn, Fe) double perovskites—Candidate anode materials for SOFCs. *Funct. Mater. Lett.* **2016**, *9*, 1641002. [[CrossRef](#)]
26. Zheng, K.; Świerczek, K.; Zając, W.; Klimkiewicz, A. Rock salt ordered-type double perovskite anode materials for solid oxide fuel cells. *Solid State Ion.* **2014**, *257*, 9–16. [[CrossRef](#)]
27. Zheng, K.; Świerczek, K.; Bratek, J.; Klimkiewicz, A. Cation-ordered perovskite-type anode and cathode materials for solid oxide fuel cells. *Solid State Ion.* **2014**, *262*, 354–358. [[CrossRef](#)]
28. Zheng, K.; Świerczek, K.; Polfus, J.M.; Sunding, M.F.; Pishahang, M.; Norby, T. Carbon Deposition and Sulfur Poisoning in $\text{SrFe}_{0.75}\text{Mo}_{0.25}\text{O}_{3-\delta}$ and $\text{SrFe}_{0.5}\text{Mn}_{0.25}\text{Mo}_{0.25}\text{O}_{3-\delta}$ Electrode Materials for Symmetrical SOFCs. *J. Electrochem. Soc.* **2015**, *162*, F1078–F1087. [[CrossRef](#)]
29. Liu, Q.; Dong, X.; Xiao, G.; Zhao, F.; Chen, F. A Novel Electrode Material for Symmetrical SOFCs. *Adv. Mater.* **2010**, *22*, 5478–5482. [[CrossRef](#)] [[PubMed](#)]
30. Li, H.; Zhao, Y.; Wang, Y.; Li, Y. $\text{Sr}_2\text{Fe}_{2-x}\text{Mo}_x\text{O}_{6-\delta}$ perovskite as an anode in a solid oxide fuel cell: Effect of the substitution ratio. *Catal. Today* **2016**, *259*, 417–422. [[CrossRef](#)]
31. Goodenough, J.B.; Huang, Y.-H. Alternative anode materials for solid oxide fuel cells. *J. Power Sources* **2007**, *173*, 1. [[CrossRef](#)]
32. Zheng, K.; Świerczek, K. Evaluation of W-containing $\text{Sr}_{1-x}\text{Ba}_x\text{Fe}_{0.75}\text{W}_{0.25}\text{O}_{3-\delta}$ (x = 0, 0.5, 1) anode materials for solid oxide fuel cells. *Solid State Ion.* **2016**, *288*, 124–129. [[CrossRef](#)]
33. Wright, J.H.; Virkar, A.V.; Liu, Q.; Chen, F. Electrical characterization and water sensitivity of $\text{Sr}_2\text{Fe}_{1.5}\text{Mo}_{0.5}\text{O}_{6-\delta}$ as a possible solid oxide fuel cell electrode. *J. Power Sources* **2013**, *237*, 13–18. [[CrossRef](#)]
34. Fang, T.-T.; Ko, T.-F. Factors Affecting the Preparation of $\text{Sr}_2\text{Fe}_{2-x}\text{Mo}_x\text{O}_6$. *J. Am. Ceram. Soc.* **2003**, *86*, 1453–1455. [[CrossRef](#)]

35. He, F.; Hou, M.; Zhu, F.; Liu, D.; Zhang, H.; Yu, F.; Zhou, Y.; Ding, Y.; Liu, M.; Chen, Y. Building Efficient and Durable Hetero-Interfaces on a Perovskite-Based Electrode for Electrochemical CO₂ Reduction. *Adv. Energy Mater.* **2022**, 2202175. [CrossRef]
36. Zheng, K. Ti-doped Sr₂Fe_{1.4-x}Ti_xMo_{0.6}O_{6-δ} Double Perovskites with Improved Stability as Anode Materials for Solid Oxide Fuel Cells. *Mater. Res. Bull.* **2020**, 128, 110877. Available online: <https://www.sciencedirect.com/science/article/abs/pii/S0025540820305882> (accessed on 1 January 2021). [CrossRef]
37. He, B.; Wang, Z.; Zhao, L.; Pan, X.; Wu, X.; Xia, C. Ti-doped molybdenum-based perovskites as anodes for solid oxide fuel cells. *J. Power Sources* **2013**, 241, 627–633. [CrossRef]
38. Du, Z.; Zhao, H.; Li, S.; Zhang, Y.; Chang, X.; Xia, Q.; Chen, N.; Gu, L.; Świerczek, K.; Li, Y.; et al. Exceptionally High Performance Anode Material Based on Lattice Structure Decorated Double Perovskite Sr₂FeMo_{2/3}Mg_{1/3}O_{6-δ} for Solid Oxide Fuel Cells. *Adv. Energy Mater.* **2018**, 8, 1800062. [CrossRef]
39. Zapata-Ramírez, V.; Mather, G.C.; Azcondo, M.T.; Amador, U.; Perez-Coll, D. Electrical and electrochemical properties of the Sr(Fe,Co,Mo)O_{3-δ} system as air electrode for reversible solid oxide cells. *J. Power Sources* **2019**, 437, 226895. [CrossRef]
40. Xie, Z.; Zhao, H.; Du, Z.; Chen, T.; Chen, N.; Liu, X.; Skinner, S.J. Effects of Co Doping on the Electrochemical Performance of Double Perovskite Oxide Sr₂MgMoO_{6-δ} as an Anode Material for Solid Oxide Fuel Cells. *J. Phys. Chem. C* **2012**, 116, 9734–9743. [CrossRef]
41. Cao, Y.; Zhu, Z.; Zhao, Y.; Zhao, W.; Wei, Z.; Liu, T. Development of tungsten stabilized SrFe_{0.8}W_{0.2}O_{3-δ} material as novel symmetrical electrode for solid oxide fuel cells. *J. Power Sources* **2020**, 455, 227951. [CrossRef]
42. Larson, A.C.; Von Dreele, R.B. *General Structure Analysis System (GSAS)*. Los Alamos National Laboratory Report LAUR 86-748 (2004). Available online: <https://11bm.xray.aps.anl.gov/documents/GSASManual.pdf> (accessed on 1 January 2021).
43. Toby, B.H. EXPGUI, a graphical user interface for GSAS. *J. Appl. Crystallogr.* **2001**, 34, 210–213. [CrossRef]
44. Li, K.; Niemczyk, A.; Świerczek, K.; Stepień, A.; Naumovich, Y.; Dąbrowa, J.; Zajusz, M.; Zheng, K.; Dabrowski, B. Co-free triple perovskite La_{1.5}Ba_{1.5}Cu₃O_{7±δ} as a promising air electrode material for solid oxide fuel cells. *J. Power Sources* **2022**, 532, 231371. [CrossRef]
45. Stroud, D. Generalized effective-medium approach to the conductivity of an inhomogeneous material. *Phys. Rev. B* **1975**, 12, 3368–3373. [CrossRef]
46. Zheng, K. Enhanced oxygen mobility by doping Yb in BaGd_{1-x}Yb_xMn₂O_{5+δ} double perovskite-structured oxygen storage materials. *Solid State Ion.* **2019**, 335, 103–112. [CrossRef]
47. Zheng, K.; Świerczek, K. Possibility of determination of transport coefficients D and k from relaxation experiments for sphere-shaped powder samples. *Solid State Ion.* **2018**, 323, 157–165. [CrossRef]
48. Crank, J. *The Mathematics of Diffusion*, 2nd ed.; Oxford University Press: New York, NY, USA, 1975.
49. Marrero-López, D.; Peña-Martínez, J.; Ruiz-Morales, J.C.; Perez-Coll, D.; Aranda, M.A.G.; Núñez, P. Synthesis, phase stability and electrical conductivity of Sr₂MgMoO_{6-δ} anode. *Mater. Res. Bull.* **2008**, 43, 2441–2450. [CrossRef]
50. Jiang, Y.; Yang, Y.; Xia, C.; Bouwmeester, H.J.M. Sr₂Fe_{1.4}Mn_{0.1}Mo_{0.5}O_{6-δ} perovskite cathode for highly efficient CO₂ electrolysis. *J. Mater. Chem.* **2019**, 7, 22939–22949. [CrossRef]
51. Kuroda, C.; Zheng, K.; Świerczek, K. Characterization of novel GdBa_{0.5}Sr_{0.5}Co_{2-x}Fe_xO_{5+δ} perovskites for application in IT-SOFC cells. *Int. J. Hydrog. Energy* **2013**, 38, 1027–1038. [CrossRef]
52. Cai, H.; Zhang, L.; Xu, J.; Huang, J.; Wei, X.; Wang, L.; Song, Z.; Long, W. Cobalt-free La_{0.5}Sr_{0.5}Fe_{0.9}Mo_{0.1}O_{3-δ} electrode for symmetrical SOFC running on H₂ and CO fuels. *Electrochim. Acta* **2019**, 320, 134642. [CrossRef]
53. Wu, Y.; Wang, S.; Gao, Y.; Yu, X.; Jiang, H.; Wei, B.; Lü, Z. In situ growth of copper-iron bimetallic nanoparticles in A-site deficient Sr₂Fe_{1.5}Mo_{0.5}O_{6-δ} as an active anode material for solid oxide fuel cells. *J. Alloy. Compd.* **2022**, 926, 166852. [CrossRef]
54. Niu, B.; Jin, F.; Yang, X.; Feng, T.; He, T. Resisting coking and sulfur poisoning of double perovskite Sr₂TiFe_{0.5}Mo_{0.5}O_{6-δ} anode material for solid oxide fuel cells. *Int. J. Hydrog. Energy* **2018**, 43, 3280–3290. [CrossRef]
55. Xie, Z.; Zhao, H.; Chen, T.; Zhou, X.; Du, Z. Synthesis and electrical properties of Al-doped Sr₂MgMoO_{6-δ} as an anode material for solid oxide fuel cells. *Int. J. Hydrog. Energy* **2011**, 36, 7257–7264. [CrossRef]